

Neurons in the Basal Forebrain Project to the Cortex in a Complex Topographic Organization that Reflects Corticocortical Connectivity Patterns: An Experimental Study Based on Retrograde Tracing and 3D Reconstruction

Laszlo Zaborszky¹, Attila Csordas¹, Kevin Mosca¹, Joseph Kim¹, Matthew R. Gielow¹, Csaba Vadasz² and Zoltan Nadasdy³

¹Center for Molecular and Behavioral Neuroscience, Rutgers University, Newark, NJ, 07102, USA, ²N. S. Kline Institute for Psychiatric Research, Orangeburg, NY 10962, USA and ³Seton Brain & Spine Institute and Department of Psychology, University of Texas, Austin, TX, USA

Address correspondence to Laszlo Zaborszky, Center for Molecular and Behavioral Neuroscience, Rutgers, The State University of New Jersey, 197 University Avenue, Newark, NJ 07102, USA. Email: zaborszky@axon.rutgers.edu

The most prominent feature of the Basal Forebrain (BF) is the collection of large cortically projecting neurons (basal nucleus of Meynert) that serve as the primary source of cholinergic input to the entire cortical mantle. Despite its broad involvement in cortical activation, attention, and memory, the functional details of the BF are not well understood due to the anatomical complexity of the region. This study tested the hypothesis that basalcortical connections reflect cortical connectivity patterns. Distinct retrograde tracers were deposited into various frontal and posterior cortical areas, and retrogradely labeled cholinergic and noncholinergic neurons were mapped in the BF. Concurrently, we mapped retrogradely labeled cells in posterior cortical areas that project to various frontal areas, and all cell populations were combined in the same coordinate system. Our studies suggest that the cholinergic and noncholinergic projections to the neocortex are not diffuse, but instead, are organized into segregated or overlapping pools of projection neurons. The extent of overlap between BF populations projecting to the cortex depends on the degree of connectivity between the cortical targets of these projection populations. We suggest that the organization of projections from the BF may enable parallel modulation of multiple groupings of interconnected yet nonadjacent cortical areas.

Keywords: cell density, large-scale corticocortical connectivity, retrograde tracing, 3D reconstruction, 3D statistical neuroanatomy

Introduction

The basal forebrain (BF) contains a diverse population of neurons, including cortically projecting cholinergic and noncholinergic neurons as well as various interneurons (Zaborszky et al. 2012). In Alzheimer's and related neurodegenerative diseases, there is a severe loss of cholinergic neurons (for reference, see Zaborszky et al. 2008). Although the original descriptions of the cholinergic system in the early 1980s acknowledged that the BF corticopetal system shows topographic organization (Saper 1984), the heterogeneous distribution of cholinergic cells, the highly variable shape of the cholinergic space across the rostrocaudal extent of the BF, and the lack of information on how the topography of the BF corticopetal projection relates to corticocortical connections have contributed to the concept in neuroscience and psychology that the cholinergic BF system "diffusely" innervates the cortex (Saper 1987). This "diffuse" hypothesis was seemingly supported by measurements of cortical acetylcholine (ACh) release using *in vivo* microdialysis techniques that did not indicate differences between cholinergic activities in different cortical regions during various behaviors (Sarter and Bruno

1997). However, the microdialysis technique used to collect cortical ACh has poor temporal and spatial resolution (Rasmusson 2000). In contrast, recent studies using enzyme-selective microelectrodes in attentional task-performing rats demonstrated that cholinergic signals manifest at different time scales in various cortical areas to support specific cognitive operations. For example, selective cholinergic activation in the prefrontal cortex (PFC) on the scale of seconds is associated with cue detection, while changes on the scale of minutes may occur on a cortex-wide scale to support the more general arousal effect of ACh (Parikh et al. 2007). These data would be hardly compatible with the concept of a diffuse organization.

Although ascending brainstem noradrenergic and dopaminergic axons contact cholinergic neurons in extensive portions of the BF, most of telencephalic afferents (cortical, amygdaloid, striatal) appear to have a preferential distribution among subregions of the BF (for ref. see Zaborszky et al. 1999, 2012; Zaborszky and Duque 2003). The PFC innervates noncholinergic neurons in the BF, including parvalbumin-containing cell populations (Zaborszky et al. 1997), suggesting some selectivity in the innervation pattern of various neurons. Moreover, our preliminary data suggest that frontal and posterior cortical areas occupying similar mediolateral positions receive input from partially overlapping cell populations in the BF. On the other hand, topographically noncorresponding frontal and posterior cortical areas receive projections from a nonoverlapping pool of neurons in the BF (Zaborszky et al. 2002). The aim of this study was to test, on a limited set of corticocortical connections, the hypothesis that overlapping subpopulations of BF neurons project to interconnected cortical areas.

In the present study, small amounts of Fluoro-gold (FG) and Fast Blue (FB) retrograde tracers were deposited into frontal and posterior cortical areas at various mediolateral locations in rats. Retrogradely labeled cholinergic and noncholinergic neurons were mapped in the BF. Additionally, retrogradely labeled cells in posterior cortical areas projecting to various frontal/prefrontal areas were mapped, and all cell populations were combined in the same coordinate system. Using computational methods, the spatial and numerical relations of the various BF projection cell populations were determined and the projection "strength" (defined as the number of cortical projection neurons) among the cortical targets of the BF cell populations was characterized. Here, we report that not only does the BF corticopetal system show a remarkably inhomogeneous organization, but this organization is also reflected in the corticocortical connections, so far unremarked upon and thus unexplained. Our studies suggest that the cholinergic and

noncholinergic projection to the neocortex is not diffuse, but instead, is organized into segregated or overlapping pools of neurons that may transmit information from specific locations from the BF to subsets of cortical areas that are themselves interconnected. The observation that projections from the BF to cortical areas reflect corticocortical connectivity patterns is very similar to findings related to corticostriatal projections (see recent discussion by Calzavara et al. 2007) and thus may indicate a broader principle of forebrain organization.

Materials and Methods

Animals and Surgical Procedure

All experiments were performed in accordance with the US Public Health Service Policy on Humane Care and Use of Laboratory Animals, the National Institutes of Health *Guidelines for the Care and Use of Animals in Research*, and were approved by the Rutgers University Institutional Review Board. Forty-eight adult male Sprague-Dawley rats (250–275 g) were used in this study. The animals were anesthetized with i.p. injection of a mixture of ketamine (40 mg/kg) and xylazine (5 mg/kg).

Paired Injection in Frontal and Posterior Cortical Areas

In the first set of experiments (E1), animals ($n = 26$) received retrograde tracer injections at 2 different cortical sites along the rostrocaudal axis. The retrograde tracer FG (2.0% FG in 0.9% saline) was iontophoretically injected, with 8 μ A DC current 7 s, on/off for 15 min, and 0.3 μ L FB (2.0% FB in 0.9% saline) was pressure-delivered with a Hamilton microsyringe (via 30- μ m tip-diameter glass micropipettes). Each subject received a single iontophoretic injection of FG into the frontal cortex. The second, FB injection was placed into caudal neocortical areas. Injection cases where the caudal tracer deposits were in the same relative mediolateral locations as the frontal injection was called “coregistered” cases, injections that were in incongruent topographical locations were called “noncoregistered” cases. After 7 days of survival, the animals were given an overdose of urethane. They were then briefly perfused transcardially with physiological saline, followed by 500 mL of cold fixative consisting of 4% paraformaldehyde and 15% saturated picric acid in phosphate buffer (0.1 M PB, pH 7.4). After perfusion, the brains were removed and postfixed overnight in the same fixative. Brains were cryoprotected in 30% sucrose. Subsequently, brains were cut into 8 series of 50- μ m-thick coronal sections on a sliding microtome. Every eighth section was stained for choline acetyl transferase (ChAT) using a monoclonal rat anti-ChAT antibody (Boehringer-Mannheim) and FITC-conjugated antirat secondary antibody (Vector). Following the immunostaining, the sections were coverslipped with Vectashield[®]. Cholinergic and noncholinergic projection neurons in the BF were mapped. Cortical projections were not evaluated because the caudal tracer injections obscured many of the labeled cells projecting to the rostral injection sites.

Paired Retrograde Tracer Injections into Frontal Cortical Areas

In the second set of experiments (E2), each animal ($n = 22$) received adjacent injections of FG and FB retrograde tracers into various mediolaterally located areas of the frontal cortex, ~ 3.7 mm anterior to bregma. We used the same anesthesia for these operations and the same method of tracer delivery as described above. After 7 days of survival, the animals were perfused, postfixed, and the brains were cut as described above. Subsequently, 50- μ m thick coronal sections were cut on a sliding microtome. Every eighth section (representing 1 in 8 series) was mounted and coverslipped with DPX (BDH Chemicals, Ltd). This series of sections (E2) was not processed for ChAT immunostaining. Retrogradely labeled cells in the BF and in the cortex projecting to these frontal injection sites were mapped.

Data Acquisition

By using a Zeiss epifluorescent microscope (Axioscop) with appropriate filter set, the FB and FG-labeled projection neurons (exciter/barrier

filter set 365/418) and the FITC-labeled (FITC exciter/barrier filter set 450–490/520) cholinergic neurons could be separately visualized in the same section. Maps of labeled cells were created from every 8th section with a $\times 20$ objective using an interactive computer system connected to the microscope equipped with the NeuroLucida[®] software package (MicroBrightField, Inc.). Fiducial markers were mapped with a $\times 5$ objective.

3D Visualization, Warping, the VRB Program

The NeuroLucida[®] files created by the data acquisition procedure were processed for further analysis and 3D reconstructions using Micro3D software (Oslo Research Park, Norway). In order to compare data from several brains, each with multiple injection sites, each map of labeled cells was visually aligned to the corresponding map of a “master” brain with the aid of surface contours and fiducial markers, including the corpus callosum, anterior commissure, internal capsule, stria medullaris, stria terminalis, and fornix. To create a maximum fit, an interactive procedure was used, including translation, rotation and shrinkage corrections along the X-, Y-, and Z-axes. To provide data transformation capabilities such as warping, flexible analysis, and 3D visualization, we developed a custom made software package, the VRB program (<http://www.virtualratbrain.org/>). In addition to warping and overlap analysis tools, we implemented the “bubble clustering” algorithm in the VRB program (Nadasdy et al. 2010). The center of gravity (COG) of a neural population was determined using the clustering program. The distance between 2 COGs was defined as the Euclidean distance in Cartesian coordinates $\sqrt{x^2 + y^2 + z^2}$.

Overlap Analysis

The degree of overlap between 2 neuronal populations was estimated by subdividing individual sections into an array of $500 \times 500 \times 50$ μ m voxels (unit volumes) and counting the number of digitized coordinate pairs (cells) per voxel. This algorithm was designed originally by Strick and colleagues (He et al. 1993) and implemented within the Micro3D program on individual sections only. To filter data for solitary cells, only voxels containing 2 or more cells were included. The degree of overlap between the 2-cell populations was quantified as the percentage of overlapping voxels that contain both population 1 and 2 at or above threshold relative to voxels that contained only population 1 or population 2 at or above threshold. The data that was analyzed using the Micro3D program for overlap analysis was later reanalyzed with the VRB program, allowing for 3D analysis of a stack of sections.

Databases and Statistical Considerations for Overlap Analysis and Correlation between Neuronal Populations

Statistical methods were used to analyze properties of a large pool of BF cell populations that were identified by their 3D coordinates in the virtual “master” brain. These cell populations were derived from the individual experiments, and were characterized by their retrograde tracer label and/or ChAT antibody staining. Once the cells were imported into the virtual master brain, properties of not only the combinations of paired injections from the experiments, but those of all virtual combinations of individual retrograde tracer injections could be analyzed. We created 3 databases: Database 1 (D1) contained 9 posterior (FB) and 9 frontal (FG) injections from experimental group E1, and BF cells projecting to these 18 targets were characterized by their retrograde tracer label and ChAT immunoreactivity. This database served to compare the overlap of various corticopetal projection populations in the BF (Fig. 5). Database D2 derived from the 3 brains from experimental group E2 with corticocortical projections to the 5 frontal deposits together with the mapped basalocortical cells to these 5 frontal cortical targets. In addition, we warped into this database BF cells that project to 9 FB posterior cortical injection targets from experimental group E1. This database served to correlate BF overlap of projection populations to the 9 caudal and 5 frontal sites with corticocortical cells projecting from the 9 posterior FB locations to the 5 frontal sites (“cortical connectional strengths”). Figure 9 explains the procedure of extracting corticocortical cells within the 9 posterior injection volumes from the total corticocortical populations, and the

upper panel in Figure 11 schematically displays the analysis. BF projection neurons were characterized in D2 only by their tracer, FG or FB. Finally, database D3 contained corticocortical cells that projected to the 5 frontal cases from experimental group E2 and BF cells that projected to 9 frontal (FG) and 9 caudal (FB) injection sites from experimental group E1. The lower panel in Figure 11 explains how the number of corticocortical cells projecting from the 9 caudal FB sites to their frontal FG counterparts were computed. This database served to correlate the BF overlap of cholinergic and noncholinergic projection populations to frontal and posterior targets with corticocortical cells projecting from the 9 posterior FB sites to the frontal sites. BF projection neurons were characterized by their tracer (FG or FB) and transmitter content (ChAT positive or noncholinergic) in this database. Equality of population sample variances was investigated using Levene's test. *t*-Tests were used for comparisons of overlap between registered and nonregistered combinations (cases). For correlation analysis, Pearson's product-moment and the Spearman's nonparametric correlation tests were employed as implemented in the SPSS statistical software package [ver. 13 for *t*-test]. For all tests, $P < 0.05$ was accepted as statistically significant.

Nomenclature and Atlas Registration

After mapping retrogradely labeled cells, the coverslips were removed and sections were stained with Nissl to identify cortical cytoarchitectonic areas. Images of the Nissl-stained sections were overlaid with the appropriate mapping files using the NeuroLucida® “virtual slice module” (Fig. 8) and, manually warped to the Adobe Illustrator® files provided with the Paxinos–Watson atlas (5th edition, 2005). In this text we try to adhere to the nomenclature adapted by Paxinos and Watson (2005); however, to make easier comparison to various terms used in the literature, we list in parentheses other terms as well. For review of cortical terminology, see Table 1 in Lysakowski et al. (1989).

Location of Cortical Injection Sites

Figure 1 schematically displays all injection sites that were analyzed in detail, at their largest extent and projected onto the appropriate Paxinos–Watson atlas plates. Panels in the upper row of Figure 1 display the location of injections that received adjacent injections of 2 different retrograde tracers into various mediolaterally located frontal areas (E2 experimental group). The middle and lower panels in Figure 1 show the topography of 9 cases with paired injections that were delivered into frontal and posterior cortical areas at similar

mediolateral but different rostrocaudal locations (using identical case numbers; experimental group E1). As injections often crossed multiple cytoarchitectonic zones, Table 1 summarizes the injection data and Figure 10 displays the percentage proportions of individual cytoarchitectonic areas represented within each injection used for further analysis. In the text, we refer to the individual injections with their case number and the tracer used.

Results

Gross Topography of Corticopetal Cells in the BF

Figure 2 shows 3D maps that were composed from several brains, displaying the general topography of cholinergic (left column) and noncholinergic (right column) neurons projecting to various cortical areas. Each target (marked with different colors) apparently receives projections from a band of cells situated along a considerable rostrocaudal extent of the BF. In general, the topography of these bands in the BF corresponds to the mediolateral location of their cortical targets. In addition, this visualization reveals a striking topography, with more laterally located targets in the frontal cortex receiving their input from more caudal levels of the BF. Panels A and B show the pattern of projections to frontal cortical regions, panels C and D to more caudal cortical regions. Similar to projections targeting the frontal cortex, retrogradely labeled cells innervating more posterior cortical areas are organized according to a mediolateral topography. This topographical principle is somewhat blurred when more injections are added (panels E and F), although the basic pattern, (rostromedial/caudolateral) holds.

Ratio of Cholinergic/Noncholinergic Projection Neurons: Double Labeling

Supplementary Table S1 summarizes the number of cholinergic and noncholinergic projection neurons in the individual cases. To make a more realistic comparison between cases, we expressed the number of labeled BF cells per unit area of the cortical injection site. Apparently, the ratio of cholinergic to noncholinergic projection neurons systematically varies according to the cortical target area: this value is lower in frontal (on the average 0.3) than in posterior cortical areas (0.6). Supplementary Table S1 also summarizes the number of double-labeled cells, that is, cholinergic and noncholinergic cells that project to both frontal and posterior cortical areas. On the average, only about 3% (0.3–8.0%) of all noncholinergic, and 3% (0–5.8%) of cholinergic neurons project both to a frontal and a posterior site. A differential cholinergic innervation of various cortical areas (Mesulam et al. 1986; Lysakowski et al. 1989; Descarries et al. 2004) is supported to some extent by the higher number of BF cholinergic neurons projecting to medial prefrontal cortex (mPFC), as compared to cholinergic projection neurons to the S1 cortex (14.5 vs. 9.0/10⁶ μm²; data computed from Supplementary Table S1).

Comparison of Overlap Between Various Projection Populations in the BF

We computed and visualized the local overlap of cell populations in the 3D data by applying a uniform criterion of overlap/segregation of neurons across voxels of the entire BF volume, which was divided into 500 × 500 × 50 μm spatial units. Table 2 provides a case-by-case comparison of the 9

Table 1

List of injection cases, in parentheses percentage values refer to fraction of injection surfaces that represent specific cytoarchitectonic zones according to the Paxinos rat atlas

Case	Tracer	Injection site
28FG	Fluoro-gold	Pr ventral (24%), IL (18%), Vo (14%), Mo (11%), Dp, ventral Cl
28FB	Fast Blue	Pr dorsal (38%), M2 (37%), Cg1 (21%),
42FG	Fluoro-gold	M2 rostral (65%), rostromedial M1 (21%)
42FB	Fast Blue	M1 rostral (42%), S1j (35%); Fr3 (13%), rostralateral M2,
46FB	Fast Blue	Aid (41%), Aiv, Di, ventral S1j
12FG	Fluoro-gold	M1 rostral (73%), Fr3 (16%), Dorsal S1j,
13FG	Fluoro-gold	M1 rostral (86%), S1j, Fr3,
40FG	Fluoro-gold	M1 rostral (75%), M2 rostral (15%), Fr3
54FG	Fluoro-gold	Pr (56%), IL (30%), Cl
34FG	Fluoro-gold	IL (48%), Pr (36%)
33FG	Fluoro-gold	IL (25%), Vo (24%), Pr (14%), Mo (13%), DP (11%), Cl
71FG	Fluoro-gold	Pr (71%), Cg1 (26%)
77FG	Fluoro-gold	Lo (49%), Aiv (36%), Aid (14%),
78FG	Fluoro-gold	Lo (32%), Aid (31%), Aiv (30%)
12FB	Fast Blue	S1ul (83%), S1d (17%)
13FB	Fast Blue	S1b (62%), S1ul (38%),
40FB	Fast Blue	S1f (65%), S1sh (19%), S1t (13%)
34FB	Fast Blue	M1 caudal (92%), M2 caudal (8%)
33FB	Fast Blue	M2 caudal (80%), M1 caudal (20%),
54FB	Fast Blue	Rs (78%), M2 caudal (18%)
71FB	Fast Blue	Gi (45%), Di (23%), Aip, Ec, Prh
77FB	Fast Blue	Aip (50%), Prh (19%), Pir (12%), Ent (11%)
78FB	Fast Blue	Aip (46%), Ec (26%), Prh (22%)

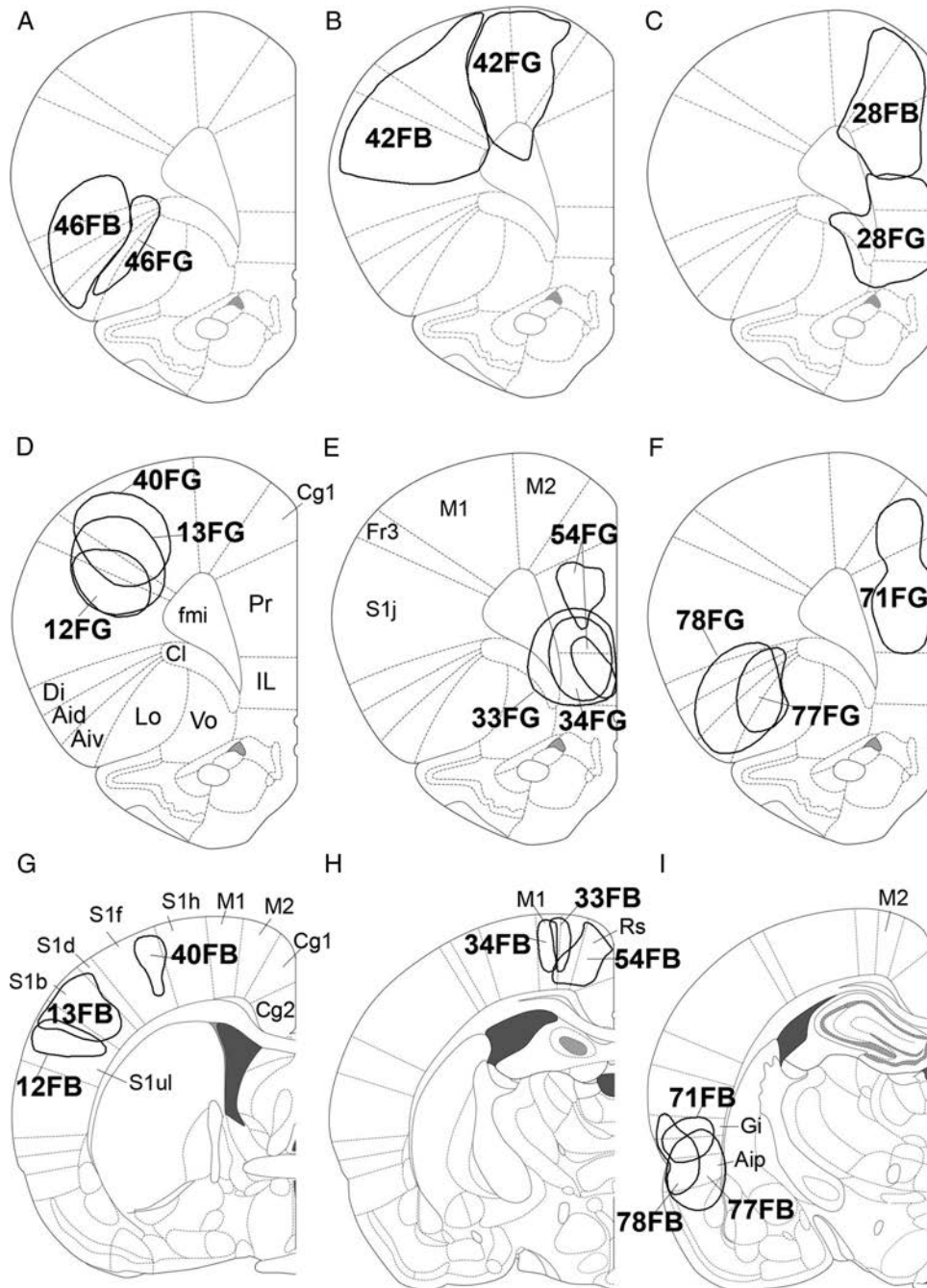


Figure 1. Location of all injection sites projected on corresponding plates of the Paxinos–Watson atlas. *A–C:* Location of the paired frontal injections using Fluoro-gold (FG) and Fast Blue (FB) (cases, 28, 42, 46); *D–I:* Location of paired injection cases (Cases 12, 13, 33, 34, 40, 54, 71, 77, 78) in which the rostral injection (FG) and the caudal injection (FB) is deposited along the same mediolateral circumference of the cortex, except in case 71, where the rostral injection is in the medial prefrontal cortex and the caudal one is located in the perirhinal cortex. Cortical areas are labeled according to the Paxinos–Watson atlas. Aid, anterior insular dorsal; Aiv, anterior insular ventral; Aip, anterior insular posterior; Cg1, cingular area 1; Cg2, cingular area 2; Cl, claustrum; Di, dysgranular insular cortex; fmi, forceps minor; Fr3, frontal area 3; Gi, granular insular; IL, infralimbic cortex; Lo, lateral orbital cortex; M1, primary motor cortex; M2, secondary motor cortex; Pr, prelimbic cortex; Rs, retrosplenial dysgranular; S1b, S1 barrel field; S1d, S1 dysgranular zone; S1f, S1 forelimb region; S1h, S1 hindlimb region; S1j, S1 cortex jaw region; S1sh, S1 shoulder region; S1ul, S1 upper lip region; Vo, ventral orbital cortex.

experimental cases with 18 cortical injections from experimental group 1 (E1), detailing the overlap between cholinergic and noncholinergic neurons projecting to frontal and posterior cortical areas. The panels in Figures 3 and 4 illustrate a series of 2D images from 2 cases (33 and 71) displaying the distribution of voxels in which the 2 populations of noncholinergic (Fig. 3)

and cholinergic (Fig. 4) neurons are segregated or overlapped. In Case 33 with a posterior injection (33FB) at the border of M1/M2 region, and with a rostral injection (33FG) centered in the infralimbic cortex with slight encroachment upon the medial part of the orbitofrontal cortex, noncholinergic and cholinergic neurons overlap in an extended territory of the BF,

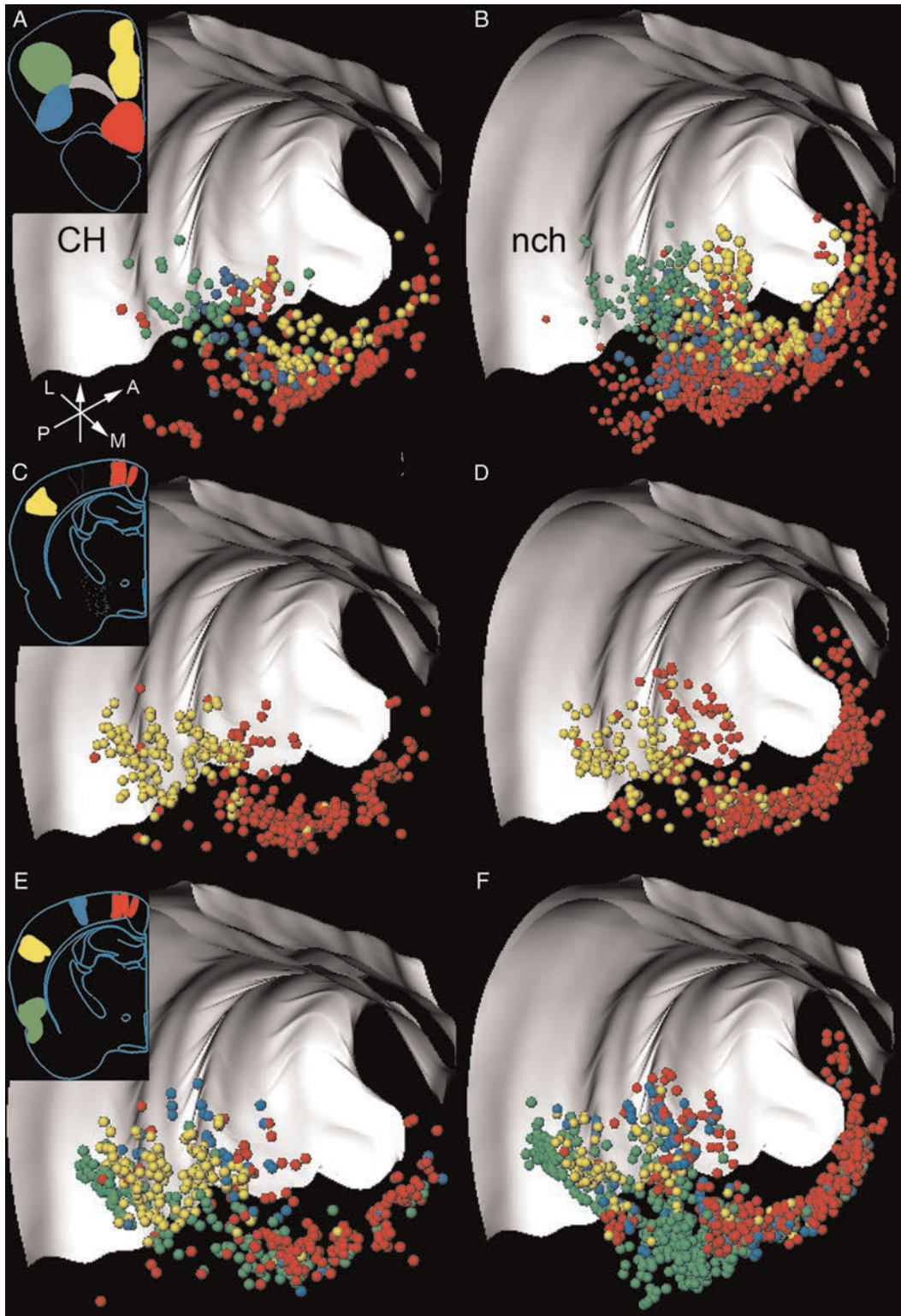


Figure 2. Comparative 3D distribution of cholinergic and noncholinergic projection neurons in the BF demonstrating the gross topography of projection. The left column represents cholinergic projection neurons only; the right column shows noncholinergic cells. *A,B*: neurons projecting to medial targets in the frontal cortex are located medially and rostrally in the BF while cells projecting to more lateral targets in the frontal cortex occupy more lateral and caudal locations in the BF. Red markers represent cells from case 34FG, yellow markers case 71FG, green markers case 13FG, and blue markers case 78FG. *C,D*: similar mediolateral topographical organization can be observed among cells in the BF that project to different mediolateral sectors in more posterior cortical areas. The red markers represent neurons that project to a medial posterior cortical area (Inj. 33FB + 34FB). The yellow markers are the representations of cells projecting to laterally located posterior cortical targets (Inj. 12FB + 13FB). *E,F*: show the distribution of cells projecting to mediolaterally located caudal cortical areas. Red cells project to the medially located M1/M2/cingulate cortical regions (Inj. 33FB + 34FB); blue cells project to the medial part of the S1 cortex (Inj. 40FB); yellow cells project to more laterally located S1 cortex (Inj. 12FB + 13FB), and green cells project to insular and perirhinal cortices (cases 71FB + 78FB). These images were generated from the initial version of database D1 using the Micro3D program. View: 45° angle. Light gray surfaces: corpus callosum and external capsule. Arrows show orientation (A, anterior; L, lateral; M, medial; P, posterior).

Table 2Comparison of overlap^a in the experimental cases^b

ID	R1CH-R2CH	nchR1-nchR2	nchR1-R2CH	R1CH-nchR2	R1-R2
54	36.00	22.09	14.67	23.26	25.58
33	17.78	13.39	9.26	21.57	22.48
34	10.00	23.60	9.41	21.95	26.04
40	6.25	35.00	12.90	24.14	29.40
13	23.53	7.32	13.95	6.67	30.18
12	9.52	12.50	6.98	22.22	32.07
78	16.67	20.00	10.43	15.36	29.62
77	10.34	23.33	16.28	6.90	28.84
71	9.50	4.80	5.77	3.95	8.90

Notes: R1 and R2 refer to the 2 tracers analyzed. The rostral tracer is always Fluoro-Gold [FG], and the caudal tracer is Fast Blue (FB). In case R1CH-R2CH, the respective cholinergic populations are compared; in nchR1-nchR2, the overlap of the 2 noncholinergic populations are investigated; under nchR1-R2CH, the FG-noncholinergic cells with the FB cholinergic population; and under R1CH-nchR2, the FG-cholinergic cell population is compared with the noncholinergic FB cells. In R1-R2, the total FG and FB populations are compared irrespective of their transmitter content.

^aVoxels of $500 \times 500 \times 50 \mu\text{m}$ were scanned for the presence of the "population 1" and "population 2" neuronal populations. For thresholding, see Materials and Methods section.

^bSee Figure 1 for location of the pairwise injection sites.

rostrally including the diagonal bands and caudally reaching the zone between the globus pallidus and internal capsule. In Case 71, the rostral injection (71FG) was placed into the anterior cingulate/prelimbic cortex, and the caudal injection (71FB) was located above the rhinal sulcus, 2–4 mm posterior to the bregma, involving granular and dysgranular insular areas. Noncholinergic and cholinergic neurons projecting to these latter 2 cortical regions show much less overlap in the BF as compared to case 33/33. The left sides of Figures 3 and 4 display 3D renderings of the distribution of retrogradely labeled cells in the BF to better appreciate the topography of overlap in case 33/33 versus segregation of cells in case 71/71.

Using NeuroLucida[®] and the VRB program we warped the 9 paired injection cases (middle-lower panels of Fig. 1) into 1 master file (database D1). The total number of combinations (k) of 2 injection sites (r) from a set of 18 injections (n), according to $k = n! / (r!(n-r)!) = 18! / (2!(18-2)!)$ is 153. After inspecting all 153 combinations, we excluded 6 combinations because no overlap was found between those pairs. In the remaining 147 combinations, we identified 8 coregistered injection combinations (cases 54, 33, 34, 40, 13, 12, 78, 77; Fig. 1) that were in the same topographical register and 139 noncoregistered combinations from which 138 were virtual cases + 1 experimental case (Case 71) in which the 2 injections were placed in noncongruent (nonregistered) parts of the frontal-posterior cortical areas. We ran the overlap analysis on each pair with several variables, comparing the location of cholinergic and noncholinergic neurons. Figure 5 is an explanatory scheme for testing overlap among BF corticopetal cell groups in various combinations. For all overlap combinations (cholinergic/cholinergic, noncholinergic/noncholinergic, noncholinergic/cholinergic, cholinergic/noncholinergic: see convention explanation in Table 2 and 3), the Levene's test for equality of variances showed no significant differences in sample variance. Assuming equal variances, we detected statistically significant ($P < 0.05$, 2 tailed) differences between coregistered and noncoregistered overlap values in all 4 combinations (Table 3). Supplementary Table S2 contains the overlapping values for all combinations.

Overlap values of all 4 combinations for the 147 cases (real + virtual combinations) were subjected to Principal Component Analysis (PCA), which was based on a correlation matrix of the

4 combinations. The correlation matrix showed that all variables were positively correlated ($P < 0.001$). There was only one major PCA component found, which explained 72.35% of the total variance with an eigenvalue of 2.89. These results suggest that the same single underlying factor is responsible for most of the variation between all 4 combinations of overlap values.

Distribution of Cortical Cells Projecting to the Frontal Cortex

To determine whether the general projection pattern of BF populations follows the large-scale organization of corticocortical connections, we generated a database of cortical projections to different mediolaterally located regions of the frontal cortex. Animals received injections of 2 different retrograde tracers, FB and FG, at various mediolateral locations in frontal/prefrontal cortical areas (experimental group E2). Three cases, involving 6 injections that cover nearly the total circumference of the frontal cortex, shown in Figure 6, were selected to demonstrate the general pattern of retrograde labeling (Cases 28, 42, and 46). For better appreciation of the 3D location of labeled cortical cells, Figure 7 displays the mapped cells in relation to outside-in and inside-out renderings of the cortical surface. Figure 8 shows the distribution of retrogradely labeled cells on selected photomontages of the same sections restained for Nissl. As cortical afferents to medial, dorsolateral, insular (sulcal), and orbital frontal areas have been described in detail in rats using both retrograde (Donoghue and Parham 1983; Isseroff et al. 1984; Reep et al. 1990, 1996; van Eden et al. 1992; Condé et al. 1995; Insausti et al. 1997; Hoover and Vertes 2007) and anterograde techniques (Miller and Vogt 1984; Swanson and Köhler 1986; Jay and Witter 1991; Insausti et al. 1997; Shi and Cassell 1998; Delatour and Witter 2002; van Groen and Wyss 2003), we only summarize our data here.

Medial Frontal Cortex (mPFC; Case 28)

In Case 28, a "ventral" (Fig. 6A–F) FG injection was centered in the infralimbic cortex, encroaching upon a small caudal part of the medial orbital cortex and dorsally the ventral part of the prelimbic cortex. The "dorsal," FB injection was located in the prelimbic/anterior cingulate cortex, and a small medial part of the motor associational cortex (M2, medial agranular frontal cortex = AGm, medial precentral cortex = PrCm).

Projections to the Ventral mPFC (Case 28FG). Projections to the ventral mPFC (case 28FG) originate primarily from 2 "stripes," one along the dorsomedial and another along the ventrolateral edges of the neopallium. The ventrolateral stripe of cells, which rostrally occupies the anterior (frontal) and posterior (parietal) agranular insular cortex, blends caudally into the perirhinal and ectorhinal areas (areas 35, 36), and reaches the lateral entorhinal cortex. A few cells along this stripe extend dorsally into the dysgranular and granular insular cortex. The cells tend to concentrate in a superficial (LII-LIII) and a deeper (LV-LVI) sheet, the latter confluent with the claustrum. The cells comprising the dorsomedial stripe occupy the cingulate cortex rostrally (Cg1 and Cg2, or areas 24a, 24b); the density of cells sharply diminishes toward the retrosplenial cortex. Additionally, a medium-density cell group is found along the M2/M1 border that continues caudally to the medial part of visual cortex (V2).

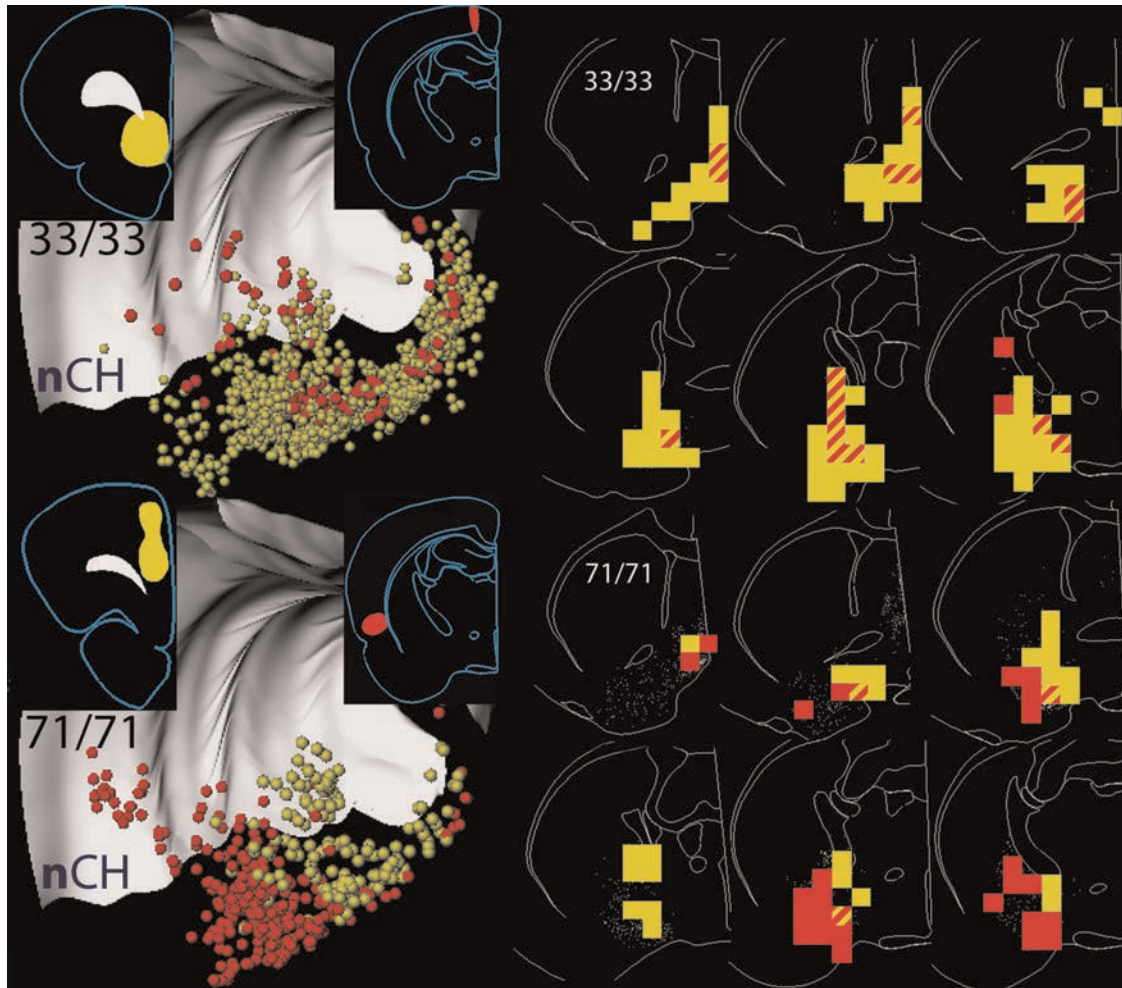


Figure 3. Overlap analysis of FG- and FB-labeled noncholinergic neurons in the BF showing 2 experimental cases with paired injections into the frontal and posterior cortex (33FG/33FB and 71FG/71FB). Each case is demonstrated by a 3D rendering and 6 coronal sections. Injection sites in the rostral and caudal cortex are shown in the upper left and right insets, on both sides of the 3D distribution map. Yellow cells project to the yellow sites, red cells to the red sites. The 6 coronal sections show the distributions of various voxels using the overlap analysis program. In the analysis, each section was subdivided into $500 \times 500 \times 50 \mu\text{m}$ voxels and the number of cells from each of the 2 populations (population "1" and population "2") was counted in each voxel. Unit spaces containing at least 2 cells of only one of these populations are marked with yellow and red, respectively; those containing at least 2 of both marker types are labeled with yellow/red stripes. Note the substantial overlap in case 33 (upper 2 rows), whereas in case 71 (lower 2 rows), few overlapping voxels are observed. The white-gray surfaces represent the corpus callosum/external capsule. These files were generated using the Micro3D program.

Projections to the Dorsal Part of mPFC (Case 28FB). Projections to the dorsal part of mPFC (case 28FB) originate primarily from a dorsal stripe of cells, although the position of cells in this stripe is shifted laterally compared to the location of cells projecting to the ventral mPFC. These cells primarily occupy the "shoulder region" of the cortex; along the M1/M2 border with a few cells in the cingulate cortex (compare red and blue cells in the upper row, panels B–F, Fig. 6). Cells projecting to the dorsal and ventral mPFC overlap in the caudal part of M2 (green cells in upper row, Fig. 6D–E). Relatively few cells project along the rhinal sulcus to the dorsal mPFC; these cells are mostly in LVI and the claustrum. In the claustrum, cells projecting to the dorsal mPFC are located mainly in the dorsal part, while the more numerous cells occupying a ventral position project to the ventral part of mPFC.

Dorsolateral Frontal Cortex (Case 42)

In case 42 (Fig. 6 middle row, panels A–F), the FG injection was centered in the secondary motor cortex (M2, PrCm, AGm),

partially encroaching upon the rostralateral part of the primary motor cortex (M1, lateral agranular cortex = AGl, Fr1, lateral precentral cortex = PrCl) between levels 3.2–4.0 mm, anterior to bregma. The FB injection was located at the same anteroposterior level in the primary motor cortex (M1), involving the jaw region of the S1 (S1j) and frontal area 3 (Fr3). The FG (red) and FB (blue) projection cells in the lateral circumference of the cortex occupy the space between the dorsomedial and ventrolateral pallial stripes described above with clear mediolateral topographic segregation.

Medial Agranular Cortex (Case 42FG). Projections to the rostral part of the M2 area originate in a large extent of the neocortex, including M2/M1, parts of the primary somatosensory cortex and the parietal association areas. Caudally, retrogradely labeled cells occupy more lateral and ventral regions of the cortex, including the secondary somatosensory (S2) and adjoining auditory regions. Scattered cells continue to be present even more caudally surrounding the fundus of the

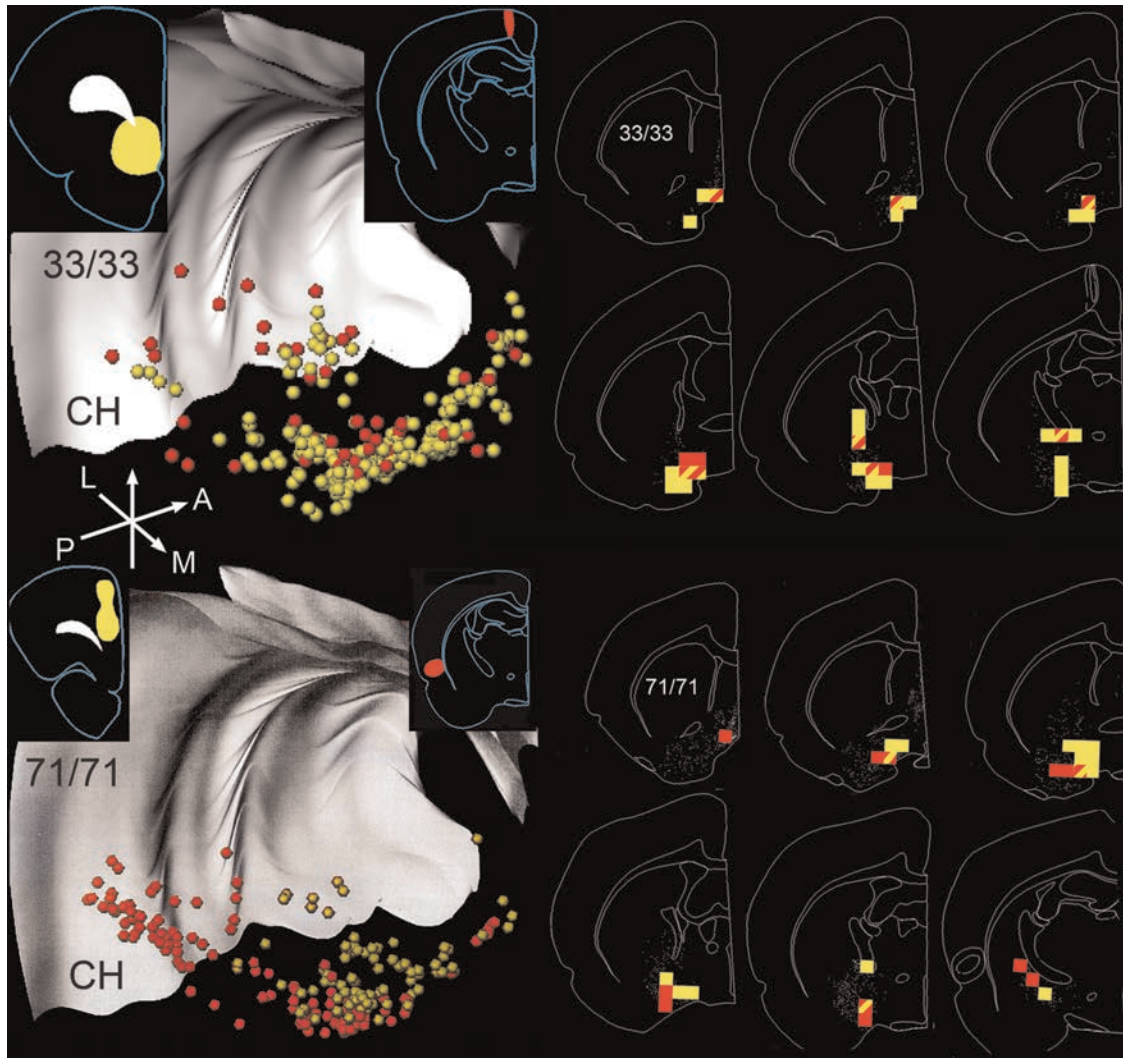


Figure 4. Overlap analysis of FG- and FB-labeled cholinergic neurons in the BF showing from the same experimental cases depicted in Figure 3 (33FG/33FB and 71FG/71FB). Injection sites in the rostral and caudal cortex are shown in the upper left and right insets, on both sides of the 3D rendering, respectively. Yellow cells project to the yellow sites, red cells to the red sites. Right maps: Overlap analysis from these 2 cases, as explained for Figure 3. Note that in case 33 (upper 2 rows), there are 8 overlapping voxels, whereas in case 71 (lower 2 rows), only 3 voxels contain the 2 populations at threshold level. Arrows show orientation (A, anterior; L, lateral; M, medial; P, posterior).

rhinal sulcus, including the insular, the ectorhinal, perirhinal, lateral entorhinal cortex, and the claustrum.

Lateral Agranular Cortex (Case 42FB). FB-labeled cells in case 42 occupy a more lateral position in the neocortex as compared to FG cells (above), that is, they are largely confined to S1 and the rostral two-thirds of S2 cortex with scattered cells in the granular and dysgranular insular cortices. In the S2 cortex there is a considerable overlap of cells projecting to both M1 and M2 areas. The claustrum also contained FB-labeled cells.

Ventrolateral Frontal Cortex (Case 46)

The lower row of panels in Figure 6 (A–F) shows the distribution of retrogradely labeled cells in case 46, where a small FG injection was located in the lateral orbital cortex and the larger FB injection involved the rostral part of the agranular insular cortex (3.8–3.2 mm anterior to the bregma). Most of FB cells were distributed throughout the entire rostrocaudal extent of the insular cortex, including its agranular, granular,

and dysgranular compartments, in a somewhat similar location to that which resulted from case 28FG, an injection site that was localized in the ventromedial PFC. Scattered cells from the insular cortex extended into the ventral part of the S2 cortex with sparse labeling throughout the S1 cortex, mainly in upper layer 5 and deep layer 6. A few labeled cells were found in layer 5 of M2, Cg1, and parietal association areas. Another group of labeled cells was located in the dorsal endopiriform nucleus and in the deep piriform cortex.

Laminar Patterns. While retrogradely labeled cells at the M1/M2 border region continuously fill all layers (Fig. 8, panel D, between arrowheads, Case 42FG), in cortical regions that possess a lamina 4 on the other hand, labeled cells characteristically concentrate in 3 layers, namely, layers 2–3, upper layer 5, and deep layer 6 (6b), while layer 4 usually is empty (see Fig. 8, panel D, S1 forelimb area; panel C, S1 upper lip, areas marked with thin lines). As compared to this trilaminar pattern, labeled cells are often condensed in an hourglass shape (Fig. 8, panel C, case 42FB, S1 dysgranular cortex: marked with

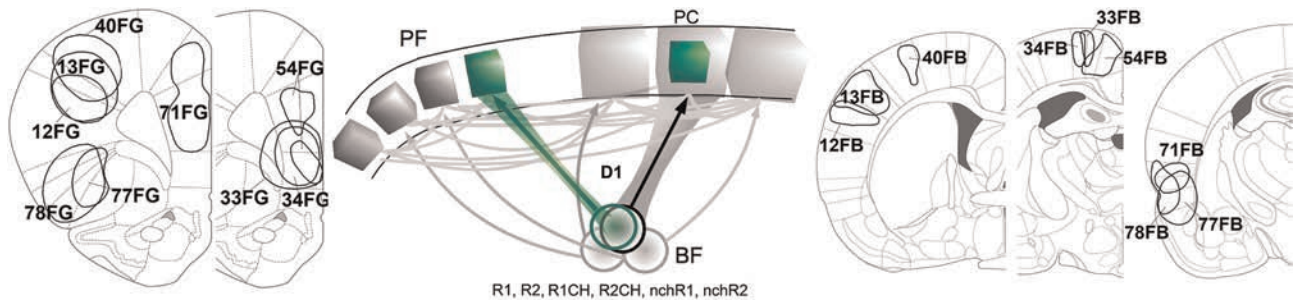


Figure 5. Schematic illustration to compute the overlap values of various experimental and virtual BF projection populations using database D1. BF overlaps between each of the topographically “coregistered” pairs are compared against all “noncoregistered” cases. Injection sites in the frontal-prefrontal cortex (PF) are shown in the left 2 maps and posterior cortical injections (PC) are displayed in the right 3 maps with their ID numbers. Green boxes represent registered pairs of injections. For the sake of simplicity, only 4 PF and 3 PC injection sites are depicted in scheme and the corresponding projection cell populations in the BF are labeled by circular symbols. The black circle represents the overlapping population projecting to 2 randomly chosen cortical targets in the explanatory scheme. This D1 database was used to compute the following overlap categories: R1CH-R2CH, nchR1-nchR2, nchR1-R2CH, R1CH-nchR2, and R1/R2. R1 and R2 represent the 2 tracers in the combinations, nch = noncholinergic, CH = cholinergic neurons. In categories R1/R2, the 2 projection neurons are mapped irrespective of their transmitter. The type of BF-labeled cells in the database is indicated. We detected statistically significant ($P < 0.05$, 2 tailed) differences between coregistered and noncoregistered overlap values in all 4 combinations (see Table 3; raw data: Supplementary Table S2).

Table 3

Comparison of overlap between “coregistered” (all experimental cases except #71) and “noncoregistered” (virtual cases + #71)

Group code	<i>N</i>	Mean	SD	<i>t</i>	<i>df</i>	<i>P</i> value
R1CH/R2CH coregistered	8	16.26	9.75	4.60	144	9.12E-06
Noncoregistered	138	5.68	6.10			
nchR1/nchR2 coregistered	8	19.65	8.56	3.53	144	0.001
Noncoregistered	138	9.93	7.53			
nchR1/R2CH coregistered	8	11.74	3.19	2.53	143	0.013
Noncoregistered	137	6.37	5.93			
R1CH/nchR2 coregistered	8	17.76	7.27	4.82	144	3.54E-06
Noncoregistered	138	6.55	6.34			

Note: R1 and R2 refer to the 2 tracers analyzed. In the experimental combinations, the rostral tracer is always Fluoro-gold (FG) and the caudal tracer is Fast Blue (FB). In the group code column, in case R1CH-R2CH, the respective cholinergic populations are compared; in nchR1-nchR2, the overlap between the 2 noncholinergic populations are investigated; under nchR1-R2CH, from one tracer the noncholinergic with the cholinergic population from the other tracer; and under R1CH-nchR2, the cell population with the opposite combination are compared. In the virtual combinations, FB injections are also compared with other FB, and FG injections with other FG injections. For the individual combinations with their overlap values, see Supplementary Table 2. SD, standard deviation; *df*, degree of freedom.

arrowheads), in which case, except for layer 1, labeled cells fill almost the entire depth of the cortex. The size of the columns is variable: typically, the outside diameter is between 0.7 and 1.4 mm, the center is 0.6–0.9 mm, and the base near the white matter is again wider, measuring between 0.5 and 1.2 mm. Rostrally, in panels *B* and *C* in the middle row of Figure 6, in addition to the heavy medial zone corresponding to the M1/M2 region, at least 2 “columns” can be recognized, where 42FB cells partially overlap with 42 FG cells. Caudally, in the S2 and auditory association areas, the labeling is wider, more diffuse, and stretches over several mm of cortical tissue. This latter labeling is confluent with retrograde cells in layers 5–6 of the perirhinal and entorhinal cortices. In certain places, such as the border between M1/M2 and the border between ventral S2 and posterior insular cortex, the heavy presence of retrogradely labeled cells obscures any clear trilaminar or hourglass shape and can be characterized as “complex” pattern.

3D Rendering of Cortical Surfaces. As seen from 3D reconstructions of the cortex in Cases 28 and 46 in Figure 7, retrogradely labeled cells in the dorsomedial (medial mesocortex

or proiso cortex) and ventrolateral part of the pallium (lateral mesocortex or periallo cortex) form more or less continuous stripes. The topographical relationship between these 2 stripes of cells is maintained over a long rostrocaudal extent. The dorsomedial stripe of cells innervates the anterior cingulate cortex dorsally and the prelimbic–infralimbic cortex ventrally. Along the rhinal sulcus, in the agranular insular, perirhinal, and entorhinal cortices, the lateral stripe of labeled cells projects to the infralimbic–prelimbic area and the rostral part of the sulcal-insular cortex. More caudally, this stripe becomes wider and extends into the ventral part of the secondary auditory cortex. This ventral stripe of labeled cells is continuous with retrogradely labeled cells in the dorsal endopiriform nucleus and deep layers of the piriform and entorhinal cortices. Owing to the spread of labeled cells in the superficial and deeper layers, the cortical regions between the dorsomedial and ventrolateral stripes are occupied by various sizes of patches, instead of the typical hourglass or columnar pattern seen in 2D coronal sections (see Case 42).

Weight of Inputs to Frontal Targets from Posterior Cortical Areas

A method of choice to test the hypothesis that overlapping populations in the BF project to interconnected cortical areas would be a combination of anterograde and retrograde tracing methods in the same animal. However, the use of at least 3 tracers (2 retrograde and 1 anterograde) and the difficulty quantifying axonal varicosities as putative synapses make this option not practical. Therefore, we modified our original hypothesis in that we test whether the measure of overlap between 2 projection populations in the BF correlates with the corticocortical connectional strength between their targets. While connectional weight is best defined at the synaptic level, we used the number of cells that project from a specific posterior location to a specific frontal area as a measure of connectional strength. We warped the 5 frontal injection cases from experimental group E2 depicted in Figure 1A–C along with their mapped corticocortical projection neurons into the same master file that contained the additional 9 posterior cortical FB injection cases from experimental group 1, displayed in the lower panels of Figure 1 (Database D2). By overlaying the FB posterior injection sites over the sections with mapped cortical

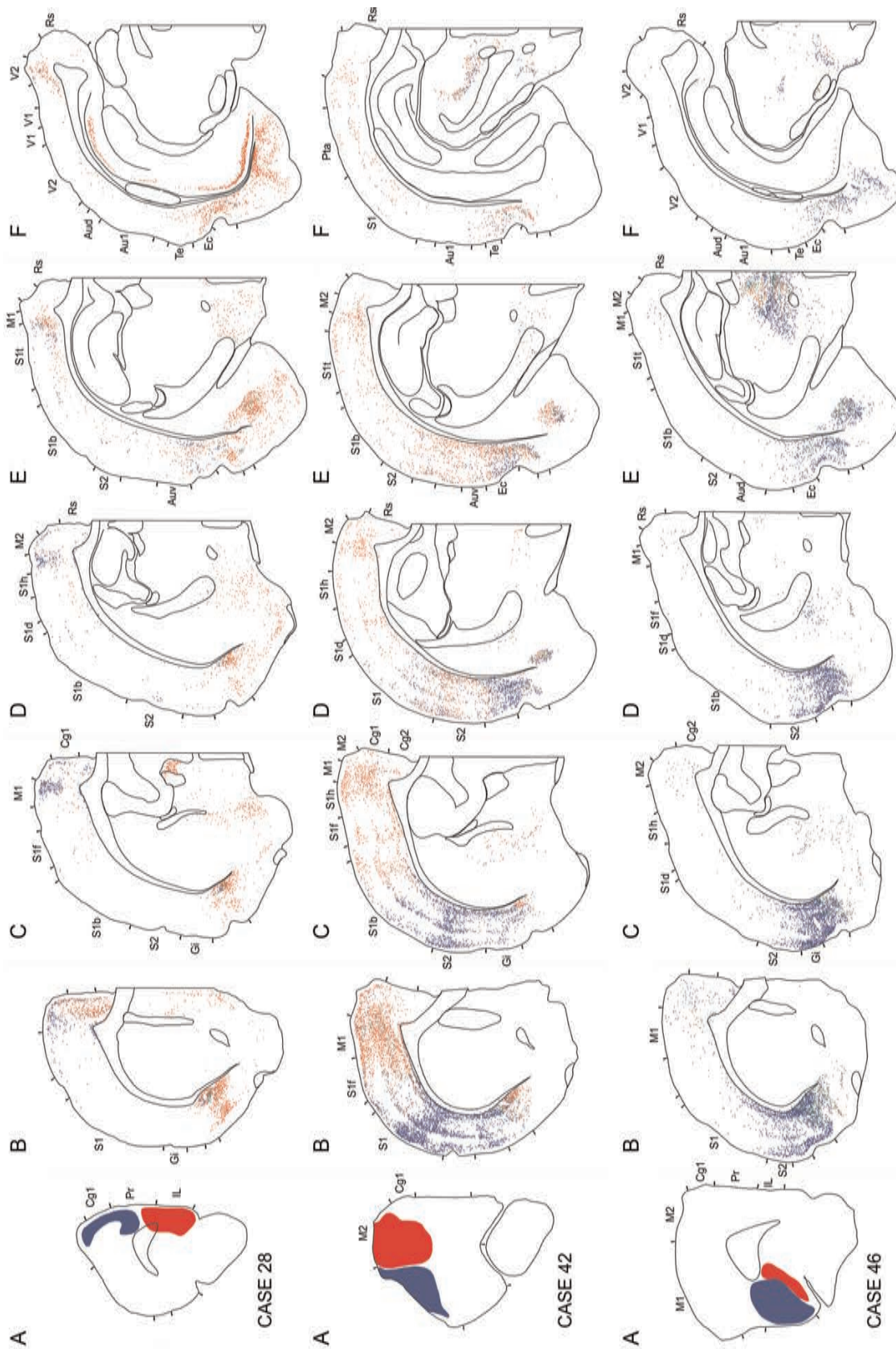


Figure 6. Maps of rostrocaudal (A–F) coronal sections showing the distribution of retrogradely labeled cells in the cortex, thalamus, and basal forebrain after injection of Fluoro-gold (FG; red) and Fast Blue (FB; blue) in the medial prefrontal cortex (case 28), in the dorsolateral frontal cortex (case 42), and in the sulcal cortex (case 46). Green dots mark double-labeled neurons. Tick marks in the cortex correspond to approximately cytoarchitecturally defined cortical areas according to the Paxinos–Watson atlas. Individual section maps can be viewed as Supplementary Figures S1–S5: case 28, panels A–F; Supplementary Figures S6–S10: case 42, panels A–F; Supplementary Figures S11–S13: case 46, panels A–F. Aud, secondary auditory cortex dorsal; Auv, secondary auditory cortex ventral; Au1, primary auditory cortex; Aid, anterior insular dorsal; Aiv, anterior insular ventral; Ap, anterior insular posterior; Cg1, cingulate area 1; Cg2, cingulate area 2; Ci, claustrum; Den, dorsal endopiriform nucleus; Di, dysgranular insular cortex; Dp, dorsal peduncular cortex; fmi, forceps minor; Ec, entorhinal cortex; Ent, entorhinal cortex dorsal; FB, Fast-blue; FG, Fluoro-gold; Fr3, frontal area 3; Gi, granular insular; IL, infralimbic cortex; Lo, lateral orbital cortex; Li-VI, cortical layers; M1, primary motor cortex; M2, secondary motor cortex; Mo, medial orbital cortex; Pr, piriform cortex; Pth, perirhinal cortex; Pta, parietal association cortex medial; Rs, retrosplenial dysgranular; S1b, S1 barrel field; S1d, S1 dysgranular zone; S1f, S1 forelimb region; S1h, S1 hindlimb region; S1i, S1 interlimb region; S1j, S1 jaw region; S1k, S1 shoulder region; S1l, S1 upper lip region; S1t, S1 trunk; S2, secondary association cortex; Vo, ventral orbital cortex; V1, primary visual cortex; V2, secondary visual cortex.

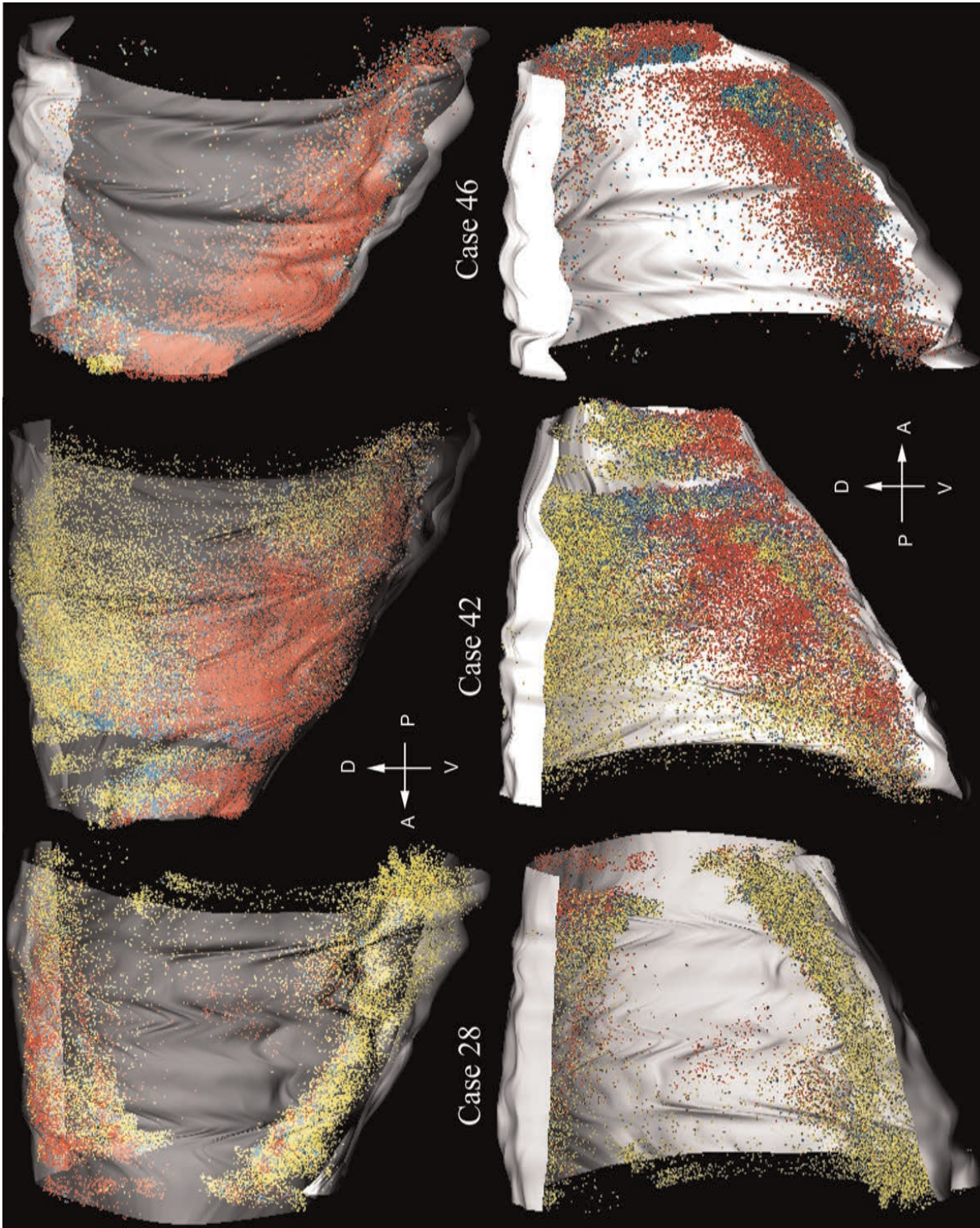


Figure 7. Distribution of retrogradely labeled cells in the cortex using 3D surface rendering tools of the Micro3D software. Upper row: outside-in view: the labeled cells are viewed through a semitransparent layer that is interpolated from the section contour outlines, lower row: inside-out view: the labeled cells are in front of a surface that represent the outside contours of the sections. The gray-white surfaces represent a rendering generated from the outlines of the mapped sections. Case numbers are indicated in the middle. Yellow dots represent FG-labeled cells that are marked with red in Figure 6; red indicates FB (marked with blue in Fig. 6), and blue indicates double-labeled cells (marked green in Fig. 6). Note the almost confluent distribution of labeled cells in large-scale multiple overlapping patches. Arrows show orientation (A, anterior; P, posterior; D, dorsal; V, ventral).

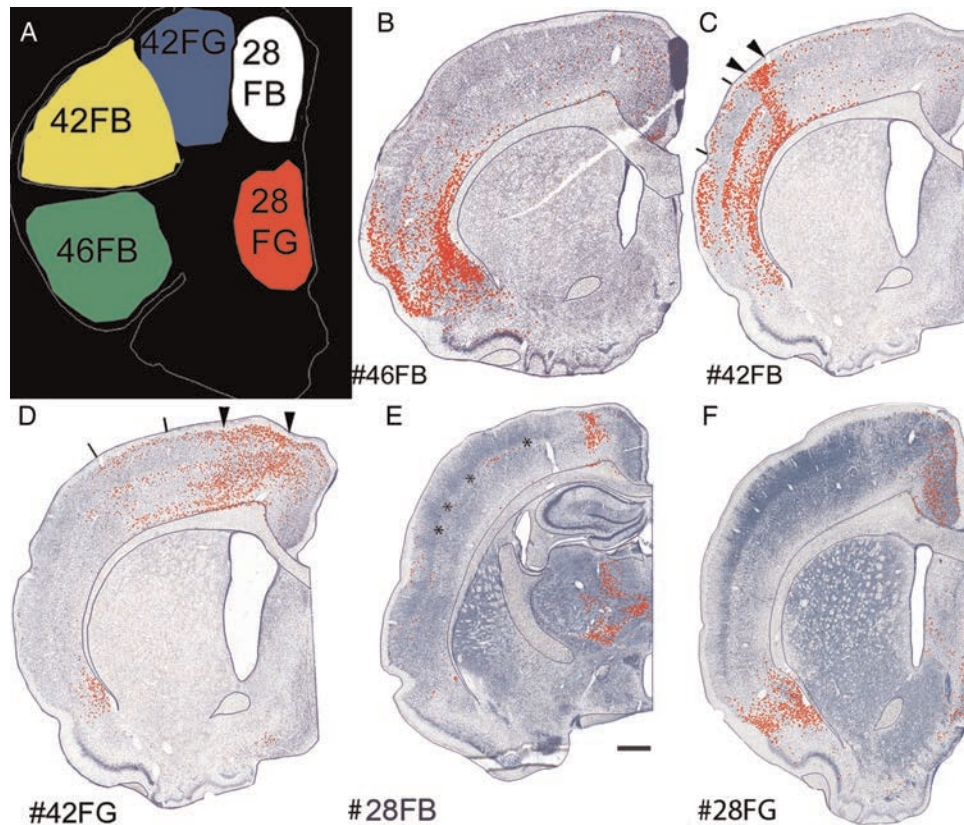


Figure 8. Distribution of retrogradely labeled cells in individual sections projected over the Nissl-image of the same section. After FB and FG cells were mapped, the sections were stained for Nissl and their images were realigned in the NeuroLucida system. Panel A shows schematically the 5 injection sites in the frontal cortex. Numbers and letters refer to case numbers shown in Figure 6 and in panel A. Note that both FB and FG cells are marked with the same red symbol for the sake of clear contrast. Labeled cells in posterior cortical areas show a trilaminar pattern (layers 2–3, upper layer 5 and 6b) between tick marks in the cortex in panels C and D, display a columnar shape (between arrowheads in panel C) or fill all cortical layers except layer 1 (complex pattern, between arrowheads in panel D). Stars in E mark the approximate location of upper layer V. Bar scale in E: 1 mm.

neurons projecting to the frontal injection sites (28FG, 28FB, 42FG, 42FB, and 46FB), we could determine the number of retrogradely labeled cells inside the area of each individual posterior injection volume. In this database, we can estimate the number of cells that project from 9 posterior locations to 5 frontal patches and in the same file we can identify the number of cells in the BF that project to the same 5 frontal and 9 posterior cortical locations in any combination. To explain this procedure, panels B–D of Figure 9 show 3 rostrocaudal levels displaying all cortical projection neurons with colors corresponding to the colors of their various targets in the frontal cortex (panel A). The lower panels (E–I) in Figure 9 depict 5 slices with 4 of the 9 posterior cortical injections; in each level, only cells projecting to the 5 frontal regions from the specified posterior injection volume are visualized.

To better appreciate the differential proportion of cells projecting from the 9 specified posterior cortical volumes to the 5 frontal targets, we created pie charts of Figure 10. Although the relation of each individual injection location to the cytoarchitecturally defined cortical areas can only be estimated (see percentage values above each pie chart and in Table 1), one can observe a systematic shift in the proportion of projection neurons to the 5 frontal targets. For example, moving counterclockwise from the medial mesocortex lateralwards (cases 54–33–34), the proportion of cells projecting to the dorsomedial PFC area is progressively higher (light gray field

occupied by injection 28FB). Also, the further lateral the injection site in the posterior cortex is (compare cases 40–13–12), the smaller the proportion of cells projecting to the rostral M2/M1 areas (blue field represented by case 42FG), and the larger the fraction of cells projecting to the laterally located M1/S1j/F3 cortical region (yellow field occupied by injection 42FB).

Comparing some of our caudal injection locations with earlier anterograde and retrograde studies (Donoghue and Parham 1983; van Eden et al. 1992; Condé et al. 1995) validates our procedure: the S1 forelimb (case 40FB) and barrel cortex (case 13FB) give rise to a negligible or very sparse projection to the infralimbic cortex/ventral prelimbic area (0 and 22 cells in Cases 13 and 40 towards 28FG) compared to a massive projection from posterior insular and perirhinal areas to the ventromedial prefrontal cortex (983 cells project from Case 77 toward 28FG) as in the cited studies. The primary motor area has been shown to project heavily to the dorsomedial part of the PFC and adjacent M2 area in these previous studies, and indeed, we found a massive projection from an area that largely corresponds to the caudal M1 area (case 34FB) to the dorsomedial PFC (360 cells to 28FB) and laterally to the M2 area (371 cells to 42FG). Interestingly, the projection from the S1 forelimb (case 40FB) was very different from the barrel (Case 13FB) and the upper lip (Case 12FB) representations that are all grouped in S1. The abrupt change in the projection from the S1 forelimb as compared to the barrel cortex suggests

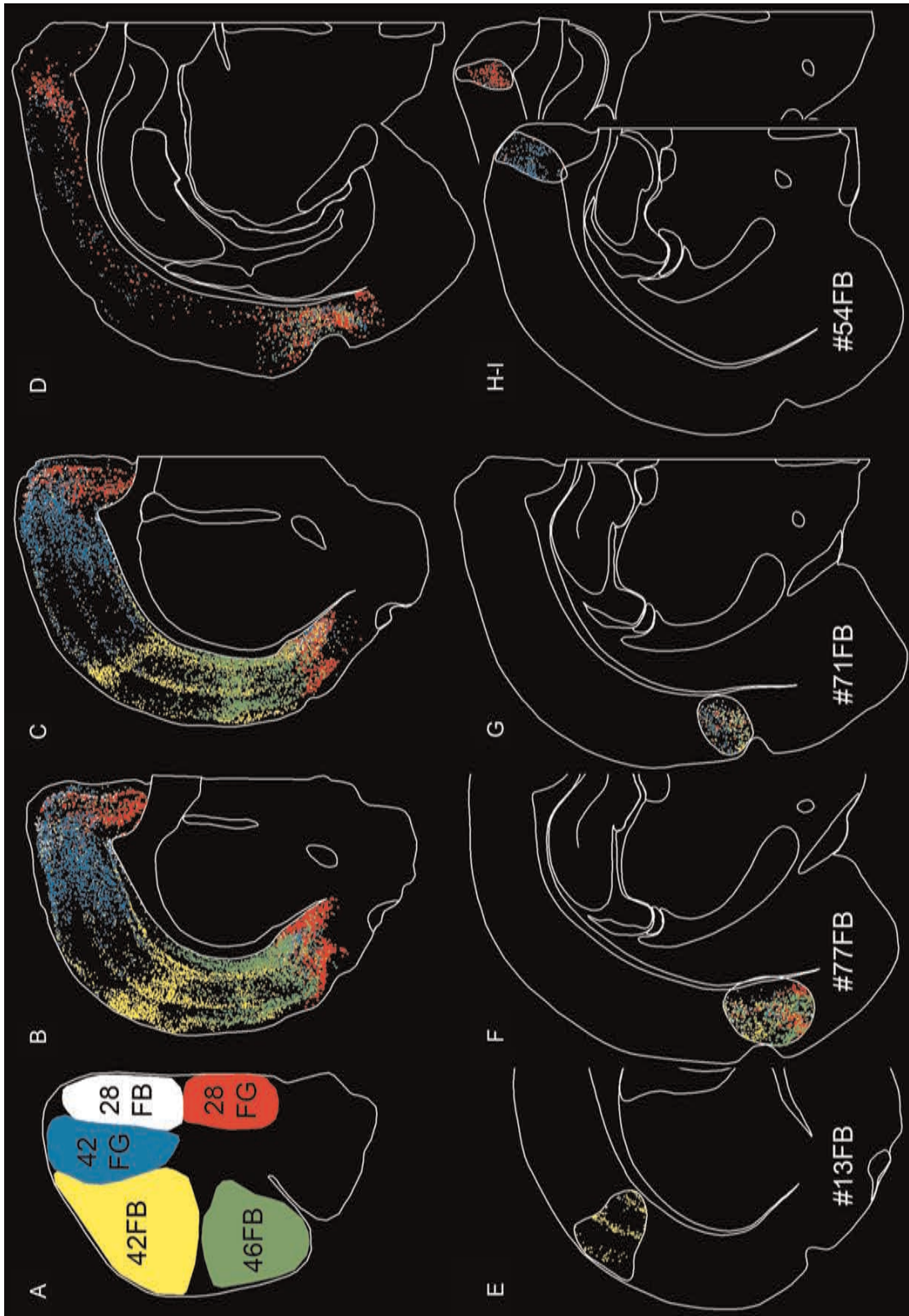


Figure 9. Extraction of cells projecting from each of the posterior cortical injection sites to the 5 frontal injection locations for creating database D2. (A) Location of injection sites in 5 cases in which cortical cells to these injection locations were mapped as shown in Figure 6. (B–D) Combined distribution of labeled cells in the cortex at 3 rostrocaudal levels resulting from the 5 frontal retrograde tracer injections. White labeled cells projecting to location 28FB are relatively few in number, located mostly along the M1/M2 border, and partially obscured by the heavy projection of blue cells to injection location 42FG. (E–I) Examples showing cells in posterior injection sites after removing cortical cells that are outside the specific injection volumes. Note that injection site 13FB (panel E), that is largely located in the S1 barrel field and upper lip representations, contain mostly yellow cells projecting to the 42FB site that corresponds to the M1 and S1 jaw cortical areas according to the Paxinos atlas. From the calculated 738 cells in the 13FB area, 36 cells project to 42FG, 9 cells to 46FB, and 4 cells to 28FB. The 2 injection volumes in the insular cortex (46FB and 46FG) contain mostly yellow cells projecting to the 42FB site, the rest (689) to the 42FG site. Within the 77FB injection volume, 983 cells project to 28FG, 898 cells to 46FB, 676 to 42FG, 535 to 42FB, and 119 to the 28FB site. In the volume of the 71FB injection 723 cells project to 42FB, 636 cells to 42FG, 352 cells to 28FG, 298 cells to 46FB, and 122 cells to the 28FB site. In case 54FB (panels H and I), the 2 sections show that the rostral part of this injection site (panel H), which is located in the retrosplenial and M2 area, contains mostly “blue” neurons projecting to the M2/M1 cortex (blue injection 42FG), but the more caudal part of the same injection case (panel I) that is located in the retrosplenial cortex is populated with “red” cells projecting to the prelimbic/mifalimbic cortex as occupied by the red target 28FG. Altogether from the total area of 54FB injection, 617 cells project to the 42FG area, 305 to 28FG zone, 46 cells to 28FB, 20 cells to 46FB, and 13 cells to the 42FB area (see data in Supplementary Table 3).

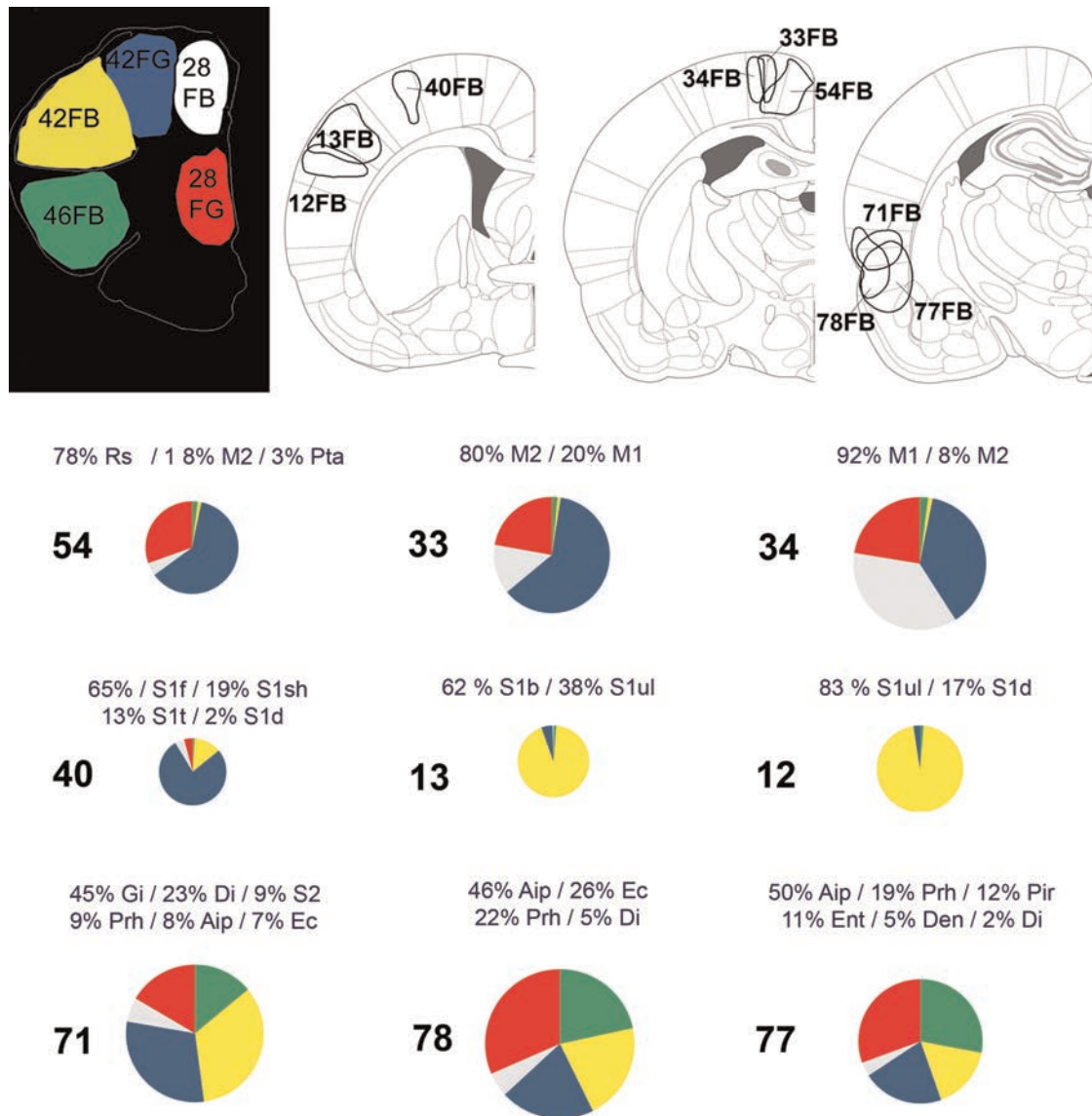


Figure 10. Pie charts showing the proportion of cells from the 9 posterior cortical locations that project to the 5 frontal target areas. Colors in the charts show the proportion of cells in the posterior injection sites (each injection is marked with the ID number of cases) that project to the specific frontal sites (color codes of frontal injections displayed in the upper left panel). The size of each chart is proportional to the number of cells within each injection volume. For cortical areas of the posterior injection sites and their frontal targets, see Table 1. Percentage numbers above each pie represent the approximate percentage of a cytoarchitectonic area within the injection based upon comparison of the surface of the individual injections with the appropriate maps in the Paxinos–Watson atlas. Aip, anterior insular posterior; Den, dorsal endopiriform nucleus; Di, dysgranular insular cortex; Ec, ectorhinal cortex; Ent, entorhinal cortex dorsal; Gi, granular insular; M1, primary motor cortex; M2, secondary motor cortex; Prh, perirhinal cortex; Pta, parietal association cortex medial; Rs, retrosplenial dysgranular; S1b, S1 barrel field; S1d, S1 dysgranular zone; S1f, S1 forelimb region; S1h, S1 shoulder region; S1ul, S1 upper lip region; S1t, S1 trunk; S2, secondary somatosensory cortex.

that topographic specificity in corticocortical connections holds true for both rat and monkey (Barbas and Rempel-Clover 1997; Medalla and Barbas 2006).

Correlation Between Overlapping BF Neuronal Populations and Cortical “Connection Strength”

To test the hypothesis that the overlap of BF neuronal populations reflects the interconnectedness of their cortical targets, we systematically compared the degree of overlap between BF populations projecting to rostral and caudal cortical areas with

the number of cells that project from the respective posterior cortical location to defined frontal cortical sites. The upper scheme in Figure 11 illustrates the type of analysis performed. Each of the posterior cortical injection cases from experimental group E1, as shown in the right 3 panels in this figure, was paired with 5 frontal retrograde injection cases from experimental group E2 in which cortical cells were mapped, resulting in 45 possible combinations (database D2). Next, we computed the percentage of overlapping voxels in the BF that contained a combination of retrogradely labeled neurons (denoted as “BF overlap”), irrespective of their transmitter

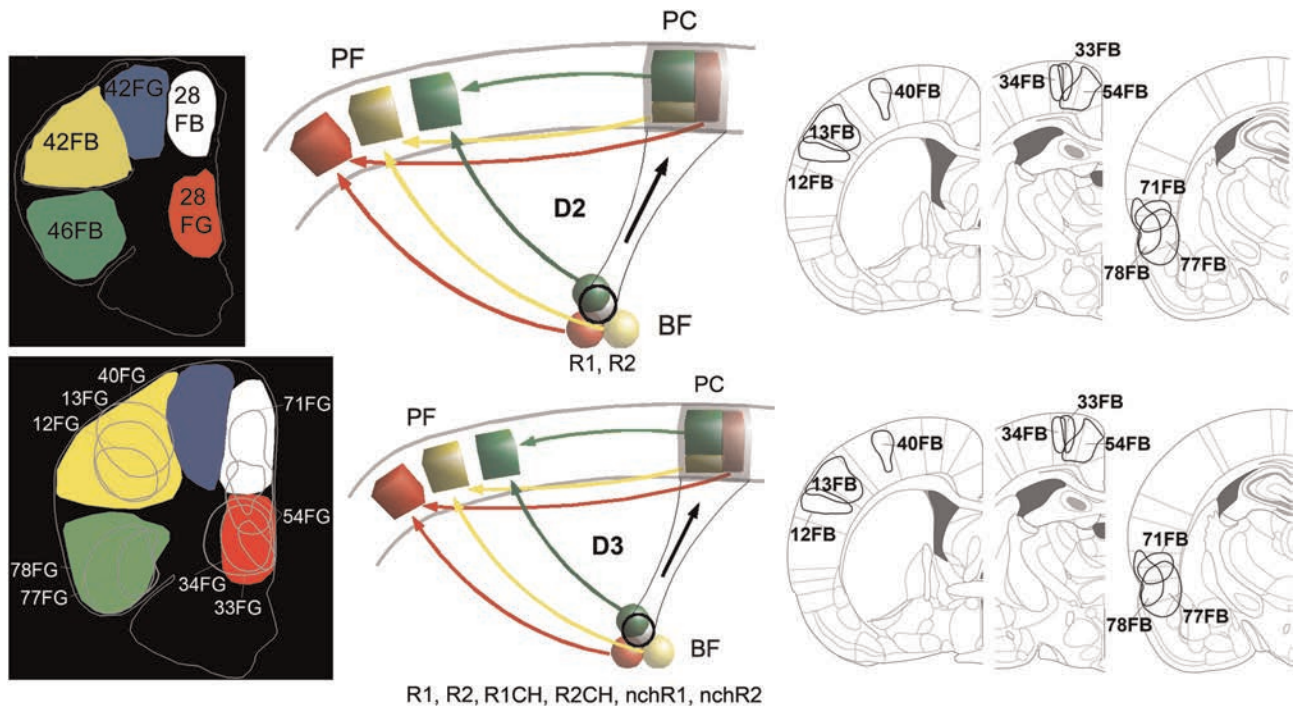


Figure 11. Schematic illustration of computing the correlation between BF overlap and cortical “connectional strengths.” Upper panel: illustration to show the correlation analysis between overlaps of BF neurons projecting to posterior (PC) and frontal cortical (PF) areas and the relatedness of their cortical targets using database D2. Left inset: location of injection sites in 5 cases for which cortical cells to these injection locations were mapped (see Fig. 6.). Right 3 maps: Location of posterior FB injection cases that are warped together with cases depicted in the left inset of this figure (Database D2). In this example, 1 PC injection site contains 3 cell groups labeled with different colors projecting to 3 PF areas. In the analysis, we compute a specific BF overlap, for example, the overlap between populations of BF cells that project to the green PF site and BF cells projecting to the PC site, and correlate this overlap value with the number of green cells within the PC injection site that project to the green PF site. We reiterate this process with all combinations. The correlation of overlap between BF cell groups projecting to the PC and PF sites and the number of cortical cells projecting from the PC to the PF site (cortical connectional strength) was significant ($P < 0.05$). This database contained only retrogradely labeled cells irrespective of their transmitter (R1 and R2). See numerical values in Supplementary Table S3. Lower panel: In database D3, we used BF overlapping values from database D1 (Supplementary Table 2); the cell numbers in the posterior FB locations (lower right 3 maps) were computed from database D2 but adjusted according to the difference between the colored injections sites (representing cases 28FG-28FB-42FG-42FB-46FB) and the gray outlined injections (representing cases 33FG-34FG-71FG-40FG-13FG-12FG-78FG-77FG). Four overlap combinations (R1/R2; R1CH/R2CH; nchR1/R2CH; and nchR1/nchR2) showed significant correlations with corticocortical connectional strength. Supplementary Tables S3–7 contain the raw data and the analysis. The type of BF-labeled cells in the database is indicated.

(grouping cholinergic + noncholinergic together), projecting to the pairs of cortical targets. Then, the BF overlap was correlated with the number of cells projecting from the 9 respective posterior FB injection sites to each of the 5 frontal injection locations, denoted as “cortical association strength.” The correlation between BF overlap and the cortical association strength (BF overlap of projection neurons irrespective of their transmitter) and number of posterior cortical cells projecting to the respective frontal cortical site) was significant ($r = 0.5843$, $P < 0.0001$, $n = 45$).

We also computed the correlation between BF overlap and cortical association strength using data set D3, comparing the 9 caudal FB injection cases (right 3 sections in the lower panel of Fig. 11) with their own frontal FG counterparts from experimental group 1 (gray outlines in the lower left panel of Fig. 11) in order to generate comparable values for cholinergic populations. As cortical cells were not mapped in experimental group E1, we used the mapped cortical projections to the 5 frontal injections from experimental group E2 as shown in Figures 6–9. For experimental group E2, we normalized cortical cell counts to reflect the size of corresponding injection sites, since the frontal injection sites did not fully match with the frontal injection locations from experimental group 1 from which we imported the cortical projection neurons, as shown schematically in the lower left panel of Fig. 11 (see raw data

and explanation for cell counting in Supplementary Tables S4–S7). We then computed the correlations between BF overlap and cortical connectional strength for all 5 combinations (R1/R2; R1CH-R2CH; nchR1-R2CH; R1CH/nchR2; R1CH-R2CH), as defined by the modified cell numbers that project from the 9 FB injection volumes to the frontal locations as delineated by injections FG13, FG33, FG34, FG40, FG54, and FG71. We found significant correlations for 3 combinations using Pearson’s 2-tail correlation coefficient. Because we hypothesized a positive correlation between cholinergic overlap (R1CH/R2CH) and connectional strength, we tested the nonparametric Spearman’s rho correlation coefficient and found significant correlation at the $P < 0.05$ level (1 tailed). See Table 4. for statistical data.

Correlation of BF Overlap with Cortical Distances of the Injection Sites

A pairwise comparison of the BF overlap values with the cortical distances between appropriate tracer injection sites showed that the cortical distance between injection sites negatively correlated with the overlap using both D1 and D2 databases (Table 4). Supplementary Tables S2 and S3 contain data for cortical injection distances as well as distance values among the COG of BF cell populations.

Table 4

Significant correlations between Bf overlap, cortical distance, and connective strength

Correlation	Group code	Correlation coefficient ^a	P value	N	Database	Supplementary Tables
Bf overlap/ connective strength	R1/R2-#cFB	0.5843	0.0001	45	D2	S3
	R1/R2-#cFB	0.3980	0.003	54	D3	S4
	nchR1/ R2CH-cFB	0.297	0.041	54	D3	S7
	nchR1/ nchR2-#cFB	0.372	0.006	54	D3	S6
	R1CH/ R2CH-#cFB	0.286 ^b	0.036	54	D3	S5
Bf overlap/ cortical distance	nchR1/ nchR2-cd	-0.202	0.012	152	D1	S2
	R1/R2-cd	-0.223	0.006	152	D1	S2
	R1/R2-cd	-0.318	0.033	45	D2	S3

Note: cd, distance between cortical FB (caudal) and the frontal injection sites;

#cFB, cortical connective strength = # of cortical FB cells projecting to each of the frontal sites.

^aPearson's 2 tailed in all cases except at ^b.^bSpearman's rho.

Discussion

The present article uses novel 3D reconstructions and numerical analyses for studying the organization of the basalocortical projection system. This analysis revealed major organizational principles between BF and corticocortical projections that can be summarized as follows: 1) Frontal and posterior cortical areas that are in topographical register receive their projection from partially overlapping volumes in the BF; 2) Topographically noncorresponding frontal and posterior areas receive their projection from nonoverlapping areas of the BF; 3) The extent of overlap between BF populations projecting to specific frontal and posterior cortical targets depends on the strength of projection of a given posterior cortical area to the specific frontal/prefrontal area. The projections from overlapping BF cell populations to interconnected cortical areas suggest that BF neurons, together with their cortical targets, form multiple functional "triangles" in which BF cell groups provide modulatory input to interacting cortical areas.

Technical Considerations

We revealed density relations between codistributed cell populations by applying a method for analyzing overlap. Similar approaches have been used by Alloway et al. (1999), Leergaard et al. (2000), and Zaborszky et al. (2005). In essence, the spatial distributions of 2 cell populations ("population 1" and "population 2") are digitized from serial sections and their overlap is quantified as the relative local density of the 2. Each digitized section is subdivided into an array of voxels (unit volumes of a given size), and the number of those cells, whose coordinates fall within the boundaries of a given voxel, is determined. The number of cells per voxel is influenced by the size of the voxels and cell count threshold criteria. A high threshold applied on small voxels would only select a few cell aggregates, which may not reflect the organization of the whole data. Conversely, a low threshold applied on large voxels would select too many voxels, which may not discriminate between spaces of different cell density. Our choice of voxel size (500 × 500 × 50 μm) was the smallest unit volume that discerns local density differences while preserving the overall structure. In our visualizations, we chose threshold

levels of 2 cells per voxel; higher threshold values would have obscured the general pattern of organization. We applied manual warping that can easily correct for distortions in the X–Y coordinates, but a more complex warping is required in the future for aligning the corresponding sections in the Z dimension. The warping method we applied was able to bring the microscopic organization of the cholinergic space into register across individual brains, based on macrostructural alignment. Because all brains in this study were of the same size, processed similarly, sliced with the same intersection distance (400 μm), and maximal caution was exercised during the cutting of tissues to avoid further misalignments, we assume that interindividual differences among the distribution of the labeled cell populations were negligible.

Cholinergic cells in the BF projecting to 2 cortical targets that are in topographical register show high overlap. On the other hand, cholinergic cells projecting to cortical areas that are not in topographical register show small overlap. One could argue that the extent of overlap or segregation of virtually combined neuronal populations depends on the precision of the warping between subjects. However, we could rule out the effect of warping since a high overlap was also observed between cholinergic neuronal populations projecting to the infralimbic and caudal M2 cortical areas that were labeled in the same subject (e.g., 33FG/33FB: 17.8%). Also, cholinergic cells projecting rostrally to the prelimbic cortex and caudally to the insular cortex (case 71FG/71FB) show only 9.5% overlap; these latter 2 targets were defined in the same animal but they were designed to be "mismatched" with respect to the injection topography.

Cholinergic and Noncholinergic Basalocortical Systems

Using specific markers for cholinergic, GABAergic, or glutamatergic neurons in combination with retrograde and anterograde tracing techniques (Zaborszky et al. 1999; Gritti et al. 2003; Hur and Zaborszky 2005; Henny and Jones 2008), it has been established that cortically projecting neurons from the BF comprise cholinergic, GABAergic, and glutamatergic neurons. These 3 transmitter-specific neuronal classes participate with different proportions in the innervation of cortical regions and could affect specific cortical cell populations in a complex manner (Hassani et al. 2009). Studies using juxtacellular labeling in combination with cortical EEG monitoring and post hoc immunocytochemistry have provided critical insight about the function of BF neuron types. Cholinergic neurons exhibit increased discharge during cortical activation (Duque et al. 2000; Manns et al. 2000; Lee et al. 2005), whereas they almost cease firing during slow-wave sleep. Thus, cholinergic cells can promote cortical activation, which underlies arousal, sensory processing, and attention.

The effect of ACh released through BF cholinergic axons in the cortex is complex due to 1) the differential regional and laminar distribution of cholinergic axons, 2) different effects on various neuronal types and cellular sites of action (cell bodies, dendrites, axons), 3) ACh effects are mediated by synaptic and volume transmission at different time scales, and 4) ACh acts through a variety of muscarinic and nicotinic receptors that are expressed differentially in pyramidal cells and in the various interneurons. It seems that the complex effects of ACh falls into line with each specific neuronal cell type's role in the information processing architecture of the cortex. In

summary, ACh increases the amplitude and signal-to-noise ratio of evoked sensory responses, has a “filtering” role by amplifying relevant inputs while suppressing weak sensory inputs, and sharpens the tuning of specific cells in sensory cortex (Eggermann and Feldmeyer 2009; Lawrence 2008; Yamasaki et al. 2010; Bell et al. 2011; Ma and Luo 2012; Medalla and Barbas 2012). Moreover, ACh elicits different types of plasticity depending on the precise time of release in the target area (Gu and Yael 2011). Finally, cholinergic modulation contributes to the activity-dependent persistent firing of pyramidal neurons in the prefrontal cortex, which has been proposed to be related to working memory (Dembrow et al. 2010).

Most noncholinergic BF neurons are GABAergic, innervating exclusively GABAergic interneurons that in turn distribute synapses onto specific locations on pyramidal neurons in the cortex. The activity of ascending GABAergic axons is associated with the timing and synchrony of large principal cell populations (Henny and Jones 2008; Hassani et al. 2009) rather than simply producing disinhibition as originally proposed (Freund and Gulyás 1991; Freund and Katona 2007). The function and precise termination of the recently described minor basolateral glutamatergic projection remains to be elucidated (Hur and Zaborszky 2005; Hassani et al. 2009; Henny and Jones 2008).

Although ACh, GABA, and glutamate released from BF corticopetal axons act on different cortical cell types through complex mechanisms, the fact that the extent of the overlap of both the noncholinergic and cholinergic corticopetal cell populations in the BF correlates with the cortical interconnectivity of their targets suggests that there is a global forebrain spatial architecture that constrains how ascending cholinergic and noncholinergic afferents originating from neighboring BF locations could contact neurons in their cortical target regions.

Overlapping Pool of Corticopetal Projection Neurons in the BF for Linked Modulation of Interconnected Cortical Areas

When comparing the spatial distribution of cholinergic or noncholinergic projection populations in the BF, it is evident that some cortical areas receive their BF projection from overlapping pools of neurons, while other cortical areas are innervated from segregated pools of neurons. The extent of overlap between 2 randomly chosen BF cell populations was found to correlate with 1) cortical topography, 2) the distance between their cortical targets, and more importantly 3) with the strength of their interconnection. Indeed, previous studies found strong interconnections between many cortical areas that are targeted by highly overlapping BF cell populations. For example, it was found that the M2/retrosplenial cortex (location of case 54FB) project heavily to the anterior cingulate/prelimbic cortex (case 71FG; see Table 1 for injection locations) as shown by Van Eden et al. (1992) and Condé et al. (1995), and indeed FBCH-54 and FGCH-71 cholinergic cell populations show the highest percentage of overlap (39%) in our database.

Because the precise spatial relationships between locations of injection sites and cytoarchitectural borders were only tentatively identified in our study, it is unclear at present whether the overlapping pools of BF neurons project to areal borders, callosal or associational columns (Zaborszky and Wolff 1982). Additional studies are necessary to determine whether the unique columnar (Rockland 2010), trilaminar or complex

distribution pattern of cortical projection neurons shown in this and previous studies does or does not correspond to specific locations of overlapping pools of neurons in the BF.

Recently, Ghashghaei and Barbas (2001) reinvestigated the projection pattern of BF to distinct areas of the prefrontal cortex (PFC) in monkeys. Comparing projections to prefrontal areas with that of other cortical areas from the Mesulam/Mufson studies (Mesulam et al. 1983), Barbas and her colleague suggested that BF projections to specific areas in the PFC originate from the same sector of the nucleus basalis (NB) that also innervates those cortical areas which receive input from the prefrontal cortex. For example, prefrontal areas 8, 46, 12, and 10 have robust connections with visual and auditory association cortices, and the same part of the posterior NB seems to innervate both auditory and visual association areas along with the cited prefrontal areas. Thus, a specific location in the NB may preferentially activate prefrontal, auditory, and visual cortices, which are linked through corticocortical connections. Our studies directly demonstrate a similar principle in rodents as far as somatosensory, somatomotor, and prefrontal cortical regions are concerned.

Cortico-Subcortical and Subcorticocortical Projections Are Organized According to Corticocortical Connectivity Pattern

Salient features of cortical connectivity in primates and rodents are beginning to emerge as testable architectonic organization principles, including topographic specificity, functional correspondence (somatotopic homology and continuity in case of somatomotor cortex), cytoarchitectonic and laminar differentiation, neural density differences, as well as distances separating cortical areas (Rockland and Pandya 1979; Barbas 1986; Goldman-Rakic 1988; Barbas and Pandya 1989; Felleman and van Essen 1991; Barbas and Rempel-Clower 1997; Hoffer and Alloway 2001; Hoover et al. 2003; Medalla and Barbas 2006; Averbach and Seo 2008; Markov et al., 2011). Knowledge of these rules allows for the investigation of whether or not cortico-subcortical connections reflect corticocortical connectivity patterns. For example, Yeterian and Van Hoesen (1978) and Yeterian and Pandya (1991) suggested that strongly interconnected cortical areas project, in part, to similar regions of the striatum. In contrast, Selemon and Goldman-Rakic (1985) showed that the striatal connections of cortically interconnected areas are organized predominantly in an interdigitating manner. Recently, Calzavara et al. (2007) extended these investigations in primates and confirmed both organizational schemes, that is, convergence and interdigitation. Although it is unclear whether the convergence in the primate striatum involves synaptic association, studies in rodents have shown that projections from interconnected parts of the M1 and S1 cortex overlap in the striatum and thalamus (Hoffer and Alloway 2001) and EM studies indeed have confirmed synaptic convergence of sensory and motor cortical afferents onto the same neuron in the rat caudate (Ramanathan et al. 2002).

Our studies clearly established that the extent of overlap between 2 randomly chosen BF projection populations correlates with corticocortical connection strength between the targets of the overlapping BF cell groups. Quantitative tracing studies in the primate cortex highlighted the prevalence of robust local connections as compared to exponential decay in the density of long-distance projection neurons (Markov et al.

2011). To correlate specific cortical target locations with specific BF sites, we registered cells projecting to a frontal target area only in a small source area in a posterior cortical area defined by a second tracer injection volume. As we did not study local cortical connections between spatial neighbors, further studies are needed to clarify whether cortical distance or functional connectivity determine the BF overlap. However, according to a study investigating the convergence of corticostriatal projections (Hoover et al. 2003), the cortical distance matters less than cortical somatotopic continuity in determining the extent of overlap in the striatum. Nevertheless, our study raises the possibility of a broader principle of forebrain organization, by showing that the organization of projections from the BF to specific cortical areas reflects corticocortical connectivity patterns.

Concluding Remarks

The integration of different sensory inputs in the brain is necessary for complex behaviors to be executed. In general, it is assumed that sensory processing in the brain goes through several steps before a decision for action is reached. In non-human primates, several polysensory association areas have been described in the parietal, temporal, frontal lobe, and in paralimbic areas (Mesulam 2000) that might subservise cross-modality integration. In the smaller rodent brains, sensory processing is simpler and goes through fewer steps before reaching the PFC. Based on the projection pattern of the BF to distinct areas of the cortex in rats, we postulate that the organization of the BF may support coactivation of distinct cortical areas that control a particular behavioral domain. Accordingly, the cortical sensory-motor processes are coordinated at several levels: 1) through corticocortical associations (e.g., Kayser and Logothetis 2007; Stein and Stanford 2008), and 2) through sub-corticocortical loops (Zikopoulos and Barbas 2006), including BF-cortical circuits. Structurally, this mechanism could involve BF “domains” that receive topographically organized input from the prefrontal cortex (Zaborszky et al. 1997). In turn, these BF “domains” project topographically to various cortical association areas.

Although the cholinergic, serotonergic, and noradrenergic projections were lumped together as diffuse ascending modulatory systems (Saper 1987), our analysis clearly shows that the BF cholinergic system has remarkable topographic specificity in the projections to the cortex. As we argued elsewhere (Zaborszky et al. 1999; Zaborszky 2002; Zaborszky and Duque 2003), restricted but topographically organized input from the prefrontal cortex to BF together with overlapping populations of BF “domains” might constitute the elementary circuit that communicate state-related activity changes from BF neurons to specific cortical areas in order to selectively modulate cognitive processes.

Author Contributions

L.Z.: conception and design of study, data analysis, interpretation, drafted manuscript. A.C.: performed all the experiments, did the histology, mapping of sections, and initial analysis. K. M. and J.K.: helped in the initial analysis. M.R.G.: created several of the databases, reanalyzed the data, ran statistics, and corrected manuscript. C.V. did the statistics. Z.N.: data analysis, interpretation, revised manuscript.

Supplementary Material

Supplementary material can be found at: <http://www.cercor.oxford-journals.org/>.

Funding

This work was supported by the National Institutes of Health (NS023945 to L.Z.).

Notes

The authors thank the 3 anonymous reviewers for their comments. *Conflict of Interest:* None declared.

References

- Alloway KD, Crist J, Mutic JJ, Roy SA. 1999. Corticostriatal projections from rat barrel cortex have an anisotropic organization that correlates with vibrissal whisking behavior. *J Neurosci.* 19:10908–10922.
- Averbeck BB, Seo M. 2008. The statistical neuroanatomy of frontal networks in the macaque. *PLoS Comput Biol.* 4:e1000050.
- Barbas H. 1986. Pattern in the laminar origin of corticocortical connections. *J Comp Neurol.* 252:415–422.
- Barbas H, Pandya DN. 1989. Architecture and intrinsic connections of the prefrontal cortex in the rhesus monkey. *J Comp Neurol.* 286:353–375.
- Barbas H, Rempel-Clower N. 1997. Cortical structure predicts the pattern of corticocortical connections. *Cereb Cortex.* 7:635–646.
- Bell K, Shim H, Chen C-K, McQuiston R. 2011. Nicotinic excitatory postsynaptic potentials in hippocampal CA1 interneurons are predominantly mediated by nicotinic receptors that contain $\alpha 4$ and $\beta 2$ subunits. *Neuropharmacology.* 61:1379–1388.
- Calzavara R, Mailly P, Haber SN. 2007. Relationship between the corticostriatal terminals from areas 9 and 46, and those from area 8A, dorsal and rostral premotor cortex and area 24c: an anatomical substrate for cognition to action. *Eur J Neurosci.* 26:2005–2024.
- Condé F, Maire-Lepoivre E, Audinat E, Crépel F. 1995. Afferent connections of the medial frontal cortex of the rat. II. Cortical and subcortical afferents. *J Comp Neurol.* 352:567–593.
- Datiche F, Cattarelli M. 1996. Reciprocal and topographic connections between the piriform and prefrontal cortices in the rat: a tracing study using the B subunit of the cholera toxin. *Brain Res Bull.* 41:391–398.
- Delatour B, Witter MP. 2002. Projections from the parahippocampal region to the prefrontal cortex in the rat: evidence of multiple pathways. *Eur J Neurosci.* 15:1400–1407.
- Dembrow NC, Chitwood R, Johnston D. 2010. Projection-specific neuromodulation of medial prefrontal cortex neurons. *Neuroscience.* 30:16922–16937.
- Descarries L, Mechawar N, Aznavour N, Watkins KC. 2004. Structural determinants of the roles of acetylcholine in cerebral cortex. *Prog Brain Res.* 145:45–58.
- Donoghue JP, Parham C. 1983. Afferent connections of the lateral agranular field of the rat motor cortex. *J Comp Neurol.* 217:390–404.
- Duque A, Balatoni B, Détári L, Zaborszky L. 2000. EEG correlation of the discharge properties of identified neurons in the basal forebrain. *J Neurophysiol.* 84:1627–1635.
- Eggermann E, Feldmeyer D. 2009. Cholinergic filtering in the recurrent excitatory microcircuit of cortical layer 4. *Proc Natl Acad Sci USA.* 106:11753–11758.
- Felleman DJ, Van Essen DC. 1991. Distributed hierarchical processing in the primate cerebral cortex. *Cereb Cortex.* 1:1–47.
- Freund TF, Gulyás AI. 1991. GABAergic interneurons containing calbindin D28 K or somatostatin are major targets of GABAergic basal forebrain afferents in the rat neocortex. *J Comp Neurol.* 314:187–199.
- Freund TF, Katona I. 2007. Perisomatic inhibition. *Neuron.* 56:33–42.

- Ghashghaei HT, Barbas H. 2001. Neural interaction between the basal forebrain and functionally distinct prefrontal cortices in the rhesus monkey. *Neuroscience*. 103:593–614.
- Goldman-Rakic PS. 1988. Topography of cognition. *Ann Rev Neurosci*. 11:137–156.
- Gritti I, Manns ID, Mainville L, Jones BE. 2003. Parvalbumin, calbindin, or calretinin in cortically projecting and GABAergic, cholinergic, or glutamatergic basal forebrain neurons of the rat. *J Comp Neurol*. 458:11–31.
- Gu Z, Yakel JL. 2011. Timing-dependent septal cholinergic induction of dynamic hippocampal synaptic plasticity. *Neuron*. 71:155–165.
- Hassani OK, Lee MG, Henny P, Jones BE. 2009. Discharge profiles of identified GABAergic in comparison to cholinergic and putative glutamatergic basal forebrain neurons across the sleep-wake cycle. *J Neurosci*. 29:11828–11840.
- He SQ, Dum RP, Strick PL. 1993. Topographic organization of corticospinal projections from the frontal lobe: motor areas on the lateral surface of the hemisphere. *J Neurosci*. 13:952–980.
- Henny P, Jones BE. 2008. Projections from basal forebrain to prefrontal cortex comprise cholinergic, GABAergic and glutamatergic inputs to pyramidal cells or interneurons. *Eur J Neurosci*. 27:654–670.
- Hoffer ZS, Alloway KD. 2001. Organization of corticostriatal projections from the vibrissal representations in the primary motor and somatosensory cortical areas of rodents. *J Comp Neurol*. 439:87–103.
- Hoover JE, Hoffer ZS, Alloway KD. 2003. Projections from primary somatosensory cortex to the neostriatum: the role of somatotopic continuity in corticostriatal convergence. *J Neurophysiol*. 89:1576–1587.
- Hoover WB, Vertes RP. 2007. Anatomical analysis of afferent projections to the medial prefrontal cortex in the rat. *Brain Struct Funct*. 212:149–179.
- Hur EE, Zaborszky L. 2005. Vglut2 afferents to the medial prefrontal and primary somatosensory cortices: a combined retrograde tracing in situ hybridization study. *J Comp Neurol*. 483:351–373.
- Insausti R, Herrero MT, Witter MP. 1997. Entorhinal cortex of the rat: cytoarchitectonic subdivisions and the origin and distribution of cortical efferents. *Hippocampus*. 7:146–183.
- Isseroff A, Schwartz ML, Dekker JJ, Goldman-Rakic PS. 1984. Columnar organization of callosal projections from rat frontal cortex. *Brain Res*. 293:213–223.
- Jay TM, Witter MP. 1991. Distribution of hippocampal CA1 and subicular efferents in the prefrontal cortex of the rat studied by means of anterograde transport of Phaseolus vulgaris-leucoagglutinin. *J Comp Neurol*. 313:574–586.
- Kayser C, Logothetis NK. 2007. Do early sensory cortices integrate cross-modal information? *Brain Struct Funct*. 212:121–132.
- Lawrence JJ. 2008. Cholinergic control of GABA release: emerging parallels between neocortex and hippocampus. *Trends Neurosci*. 31:317–327.
- Lee MG, Hassani OK, Alonso A, Jones BE. 2005. Cholinergic basal forebrain neurons burst with theta during waking and paradoxical sleep. *J Neurosci*. 25:4365–4369.
- Leergaard TB, Lyngstad KA, Thompson JH, Taeymans S, Vos BP, De Schutter E, Bower JM, Bjaalie JG. 2000. Rat somatosensory cerebropontocerebellar pathways: spatial relationships of the somatotopic map of the primary somatosensory cortex are preserved in a three-dimensional clustered pontine map. *J Comp Neurol*. 422:246–266.
- Lysakowski A, Wainer BH, Bruce G, Hersh LB. 1989. An atlas of the regional and laminar distribution of choline acetyltransferase immunoreactivity in rat cerebral cortex. *Neuroscience*. 28:291–336.
- Ma M, Luo M. 2012. Optogenetic activation of basal forebrain cholinergic neurons modulates neuronal excitability and sensory responses in the main olfactory bulb. *Neuroscience*. 32:10105–10116.
- Manns ID, Alonso A, Jones BE. 2000. Discharge properties of juxtacellularly labeled and immunohistochemically identified cholinergic basal forebrain neurons recorded in association with the electroencephalogram in anesthetized rats. *J Neuroscience*. 20:1505–1518.
- Markov NT, Misery P, Falchier A, Lamy C, Vezoli J, Quilodran R, Gariel MA, Giroud P, Ercey-Ravasz M, Pilaz LJ et al. 2011. Weight consistency specifies regularities of macaque cortical networks. *Cereb Cortex*. 21:1254–1272.
- Medalla M, Barbas H. 2006. Diversity of laminar connections linking periarculate and lateral intraparietal areas depends on cortical structure. *Eur J Neurosci*. 23:161–179.
- Medalla M, Barbas H. 2012. The anterior cingulate cortex may enhance inhibition of lateral prefrontal cortex via m2 cholinergic receptors at dual synaptic sites. *J Neurosci*. 32:15611–15625.
- Mesulam MM. 2000. Principles of behavioral and cognitive neurology. 2nd ed. New York: Oxford University Press.
- Mesulam MM, Mufson EJ, Levey AI. 1983. Cholinergic innervation of cortex by the basal forebrain: cytochemistry and cortical connections of the septal area, diagonal band nuclei, nucleus basalis (substantia innominata), and hypothalamus in the rhesus monkey. *J Comp Neurol*. 214:170–197.
- Mesulam MM, Volicer L, Marquis JK, Mufson EJ, Green CR. 1986. Systematic regional differences in the cholinergic innervation of the primate cerebral cortex: distribution of enzyme activities and some behavioral implications. *Ann Neurol*. 19:144–151.
- Miller MW, Vogt BA. 1984. Direct connections of rat visual cortex with sensory, motor, and association cortices. *J Comp Neurol*. 226:184–202.
- Nadasdy Z, Varsanyi P, Zaborszky L. 2010. Clustering of large cell populations: method and application to the basal forebrain cholinergic system. *J Neurosci Meth*. 194:46–55.
- Parikh V, Kozak R, Martinez V, Sarter M. 2007. Prefrontal acetylcholine release controls cue detection on multiple timescales. *Neuron*. 56:141–154.
- Paxinos G, Watson C. 2005. The rat brain in stereotaxic coordinates. 5th ed. Burlington (MA): Elsevier Academic Press.
- Ramanathan S, Hanley JJ, Deniau J-M, Bolam JP. 2002. Synaptic convergence of motor and somatosensory cortical afferents onto GABAergic interneurons in the rat striatum. *Neuroscience*. 22:8158–8169.
- Rasmusson DD. 2000. The role of acetylcholine in cortical synaptic plasticity. *Behav Brain Res*. 115:205–218.
- Reep RL, Corwin JV, King V. 1996. Neuronal connections of orbital cortex in rats: topography of cortical and thalamic afferents. *Exp Brain Res*. 111:215–232.
- Reep RL, Goodwin GS, Corwin JV. 1990. Topographic organization in the corticocortical connections of medial agranular cortex in rats. *J Comp Neurol*. 294:262–280.
- Rockland KS. 2010. Five points on columns. *Front Neuroanat*. 4:1–10.
- Rockland KS, Pandya DN. 1979. Laminar origins and terminations of cortical connections of the occipital lobe in rhesus monkey. *Brain Res*. 179:3–20.
- Saper CB. 1987. Diffuse cortical projection systems: anatomical organization and role in cortical function. In: Mountcastle VB, Plum F, Geiger S, editors. *Handbook of physiology: the nervous system*, Vol 5, Part 1. Bethesda (MD): American Physiological Society. p. 169–210.
- Saper CB. 1984. Organization of cerebral cortical afferent systems in the rat. II. Magnocellular basal nucleus. *J Comp Neurol*. 222:313–342.
- Sarter M, Bruno J. 1997. Cognitive functions of cortical acetylcholine: toward a unifying hypothesis. *Brain Res Rev*. 23:28–46.
- Selemon LD, Goldman-Rakic PS. 1985. Longitudinal topography and interdigitation of corticostriatal projections in the rhesus monkey. *J Neurosci*. 5:776–794.
- Shi CJ, Cassell MD. 1998. Cascade projections from somatosensory cortex to the rat basolateral amygdala via the parietal insular cortex. *J Comp Neurol*. 399:469–491.
- Stein BE, Stanford TR. 2008. Multisensory integration: current issues from the perspective of the single neuron. *Nat Rev Neurosci*. 9:255–266.
- Swanson LW, Köhler C. 1986. Anatomical evidence for direct projections from the entorhinal area to the entire cortical mantle in the rat. *J Neurosci*. 6:3010–3023.

- Van Eden CG, Lamme VAF, Uylings HBM. 1992. Heterotopic cortical afferents to the medial prefrontal cortex in the rat. A combined retrograde and anterograde tracer study. *Eur J Neurosci*. 4:77–97.
- Van Groen T, Wyss JM. 2003. Connections of the retrosplenial granular b cortex in the rat. *J Comp Neurol*. 463:249–263.
- Yamasaki M, Matsui M, Watanabe M. 2010. Preferential localization of muscarinic M1 receptor on dendritic shaft and spine of cortical pyramidal cells and its anatomical evidence for volume transmission. *J Neurosci*. 30:4408–4418.
- Yeterian EH, Pandya DN. 1991. Prefrontostriatal connections in relation to cortical architectonic organization in rhesus monkeys. *J Comp Neurol*. 312:43–67.
- Yeterian EH, Van Hoesen GW. 1978. Cortico-striate projections in the rhesus monkey: the organization of certain cortico-caudate connections. *Brain Res*. 139:43–63.
- Zaborszky L. 2002. The modular organization of brain systems. *Prog Brain Res*. 136:359–372.
- Zaborszky L, Buhl DL, Pabalashingham S, Bjaalie JG, Nadasdy Z. 2005. Three-dimensional chemoarchitecture of the basal forebrain: spatially specific association of cholinergic and calcium binding protein-containing neurons. *Neuroscience*. 136:697–713.
- Zaborszky L, Csordas A, Buhl DL, Duque A, Somogyi J, Nadasdy Z. 2002. Computational anatomical analysis of the basal forebrain corticopetal system. In: Ascoli GA, editor. *Computational neuroanatomy. Principles and methods*. Totowa (NJ): Humana Press. p. 171–197.
- Zaborszky L, Duque A. 2003. Sleep-wake mechanisms and basal forebrain circuitry. *Front Biosci*. 8:d1146–69.
- Zaborszky L, Gaykema RP, Swanson DJ, Cullinan WE, Zaborszky L. 1997. Cortical input to the basal forebrain. *Neuroscience*. 79:1051–1078.
- Zaborszky L, Hoemke L, Mohlberg H, Schleicher A, Amunts K, Zilles K. 2008. Stereotaxic probabilistic maps of the magnocellular cell groups in human basal forebrain. *NeuroImage*. 42:1127–1141.
- Zaborszky L, Pang K, Somogyi J, Nadasdy Z, Kallo I. 1999. The basal forebrain corticopetal system revisited. *Ann N Y Acad Sci*. 877:339–367.
- Zaborszky L, Van den A, Gyengesi E. 2012. The basal forebrain cholinergic projection system in mice. In: Watson C, Paxinos G, Puelles L, editors. *The mouse nervous system*. 1st ed. Amsterdam: Elsevier. p. 684–718.
- Zaborszky L, Wolff JR. 1982. Distribution patterns and individual variations of callosal connections in the albino rat. *Anat Embryol (Berl)*. 165:213–232.
- Zikopoulos B, Barbas H. 2006. Prefrontal projections to the thalamic reticular nucleus form a unique circuit for attentional mechanisms. *J Neurosci*. 26:7348–7361.